

Constraints on the total coupling strength to bosons in the iron based superconductors.

Stefan-Ludwig Drechsler^{*,1}, Helge Rosner², Vadim Grinenko⁴, Steve Johnston^{1,3}

¹ Leibniz-Institute for Solid State and Materials Research, Institute for Solid State Theory, IFW-Dresden, D-01171 Dresden, Germany

² Max-Planck-Institute for Chemical Physics of Solids, Dresden, Germany

³ Department of Physics and Astronomy, University of Tennessee, Knoxville 37996, USA

⁴ Technical University of Dresden, Institute for Solid State Physics, Dresden, Germany

Received XXXX, revised XXXX, accepted XXXX

Published online XXXX

Key words: Superconductivity, iron-based superconductors, Eliashberg-theory

* Corresponding author: e-mail: s.l.drechsler@ifw-dresden.de

Despite the fact that the Fe-based superconductors (FeSCs) were discovered nearly ten years ago, the community is still devoting a tremendous effort towards elucidating their relevant microscopic pairing mechanism(s) and interactions. At present, there is still no consistent interpretation of their normal state properties, where the strength of the electron-electron interaction and the role of correlation effects are under debate. Here, we examine several common materials and illustrate various problems and concepts that are generic for all FeSCs. Based on empirical observations and qualitative insight from density functional theory, we show that the superconducting and low-energy thermodynamic properties of the FeSCs can be described semi-quantitatively within multiband Eliashberg theory. We account for an important high-energy mass renormalization phenomenologically, and in agreement with constraints provided by thermodynamic, optical, and angle-resolved photoemission data. When seen in this way, all FeSCs with $T_c < 40$ K studied so far are found to belong to an *intermediate* coupling regime. This finding is in contrast to the strong coupling scenarios proposed in the early period of the FeSC history. We also discuss several related issues, including the role of band shifts as measured by the positions of van Hove singularities, and the nature of a recently suggested quantum critical point in the strongly hole-doped systems $A\text{Fe}_2\text{As}_2$ ($A = \text{K}, \text{Rb}, \text{Cs}$). Using high-precision full relativistic GGA-band structure calculations, we arrive at a somewhat milder mass renormalization in comparison with previous studies. From the calculated mass anisotropies of all Fermi surface sheets, only the ε -pocket near the corner of the BZ is compatible with the experimentally observed anisotropy of the upper critical field, pointing to its dominant role in the superconductivity of these three compounds.

Copyright line will be provided by the publisher

1 Introduction. The physics of the Fe-based superconductors (FeSCs), discovered first in the “precursor” low- T_c material LaFeOP in 2006 [1] and followed by the F-doped pnictide isomorphic sister compound in 2008 [2], is very rich and somewhat distinctive in comparison to other families of conventional and unconventional superconductors [3,4,5,6,7]. In particular, it is still unclear whether a single pairing mechanism with some modifications is at work in these materials (e.g. mediated by interband spin-fluctuations), or if charge and orbital fluc-

tuations or phonons also play some role. (The latter were initially excluded both theoretically by density functional theory [DFT] approaches, which ignore magnetic, orbital, and correlation effects [8], and experimentally by femtosecond time-resolved photoemission measurements [9], both yielding electron-phonon [el-ph] coupling constants $\lambda_{\text{el-ph}} \leq 0.2$.) Related questions concern how to classify the sometimes observed nodal superconducting order parameter (SCOP) as either an accidental s_{\pm} [10, 11] symmetry or as a protected d -wave symmetry [12, 13, 14]. Or,

Copyright line will be provided by the publisher

is there a change in symmetry of the SCOP from a sign-reversing to a sign-preserving character at a relatively high T_c with/without a significant intraband coupling [15, 16]?

One of the main difficulties in addressing these issues lay in the fact that superconductivity often occurs in the close vicinity of various competing and supporting (by their dynamical fluctuations) instabilities, whose microscopic origins are also not well understood. Another lies in the fact that the degree of electronic correlations in the FeSCs is not entirely established, and likely varies from material to material [17, 18]. Nevertheless, there has been tremendous progress in modeling the FeSCs, even at a quantitative level using various methods.

One commonly used approach utilizes Eliashberg-type models, where exchange bosons often identified with the interband antiferromagnetic spin fluctuations mediate pairing. Such phenomenological approaches are capable of quantitatively capturing many experimental observations [19, 20, 21, 22, 23, 24, 25, 26, 27]. The central quantity here is the so-called bosonic (or Eliashberg) spectral function denoted $\alpha^2 F_{ij}(\mathbf{k}, \mathbf{q}, \nu)$ in the case of phonons or $I^2 \chi_{ij}(\mathbf{k}, \mathbf{q}, \nu)$ in the case of spin-fluctuations. This function describes the effective spectrum and its coupling strength for the exchange bosons that mediating the pairing. (Here, i, j are band indices, which allow for inter- and intraband components.) An important quantity is the total strength of the exchange interaction, which can be quantified by integrating the uniform component of the spectral density

$$\lambda_{ij} = \int_0^\infty \frac{2d\nu}{\nu} \langle\langle \alpha^2 F_{ij}(\mathbf{k}, \mathbf{q}, \nu) \rangle\rangle, \quad (1)$$

where $\langle\langle \dots \rangle\rangle$ denotes a double Fermi surface average over the relevant bands. The band resolved dimensionless couplings λ_{ij} or the band averaged quantity $\lambda_{\text{el-b}} = \sum_{ij} \lambda_{ij} N_i(0)/N(0)$ are of fundamental interest as they can be related to the average increase in the effective mass of the carriers at the Fermi level due to the exchange of bosons. [Here, $N_i(0)$ and $N(0)$ denote the partial and total density of states (DOS) at the Fermi level, respectively.]

In this paper, we will review elements of our work supported by the German Research Foundation (Deutsche Forschungsgemeinschaft) through priority program SPP 1458 and present new high-resolution *ab initio* results for several classes of FeSCs. Our goal is to qualitatively discuss several general aspects pertaining to Eliashberg-based approaches for these materials, which has arisen from these projects. In another paper in this volume [16] we review related work examining how impurity scattering can induce changes in the symmetry of the SCOP in such models. Here, we focus on another issue, namely how measurements of renormalized thermodynamic quantities with respect to their corresponding “bare” values can be used to constrain the total electron-boson (el-b) coupling $\lambda_{\text{el-b}}$ in exchange boson scenarios. In doing so, we place restric-

tions on semi-empirical Eliashberg-based approaches used to describe the FeSCs and argue that the boson-exchange scenarios studied to date place the FeSCs in an intermediate coupling regime, with the band, averaged coupling $\lambda_{\text{el-b}} \lesssim 1 - 1.5$. The physical scenario for the hole-doped AFe₂As₂ FeSCs (A = K, Rb, Cs) given in the second part of the present paper was presented at the closing Workshop of the SPP 1458 hold in 13-17. September 2016 in Munich [28]. Details related to the van Hove singularities will be published elsewhere.

1.1 General aspects of el-el interactions. Before we begin, we make some general remarks about the el-el interaction in the FeSCs.

The phase diagrams of the FeSCs is affected by doping, pressure, strain, and disorder. But it is unclear which microscopic interactions drive the relative phases and their boundaries in the phase diagram. In this context, the proper description of correlation effects in FeSCs is one of the central and most difficult theoretical problems in the field. It is becoming more and more apparent, however, that different electron groups experience varying degrees of correlations, while the overall strength increases with hole doping [17, 18]. One is hence confronted with a complicated problem of treating two (or even three) electron liquids. Any attempt to address all of the particles and their interactions quantitatively and on an equal footing is clearly not possible at present, due to the extreme complexity of the many-body problem. Nevertheless, analyzing the superconducting and normal state properties of the FeSCs and comparing them with band structure calculations roughly identifies the Fe $3d_{xz}$, $3d_{yz}$, and $3d_{xy}$ orbitals as crucial for superconductivity, magnetism, and electronically driven nematicity.

Another related aspect is the impact of the high-energy electronic interactions, such as the local Hubbard repulsion U and Hund’s rule exchange J on the band structure. These terms are responsible for a significant overall band narrowing observed across all FeSCs at high energies, which in turn produces a sizable mass enhancement for the carriers at the Fermi level. This renormalization is most apparent in the $\sim 2\times - 3\times$ rescaling of the band structure frequently needed to produce a reasonable agreement between DFT predictions and the bands observed in angle-resolved photoemission spectroscopy (ARPES) [29], or for thermodynamic measurements such as the specific heat (see for example Ref. [22]). Interestingly, the largest mass renormalizations have been inferred for CsFe₂As₂ (Cs-122), which also has one of the lowest T_c values. Since the less correlated iron phosphides also achieve relatively small T_c ’s, it is reasonable to infer that moderate correlations are somehow favorable for superconductivity. In addition to driving large-scale band renormalizations, the electronic interactions are also believed to drive pairing in the FeSCs through the formation of antiferromagnetic spin fluctua-

tions [30,31] or possibly other electronic mechanisms [32, 33].

Electronic correlations can also influence interactions with the lattice, and it is important to realize that the theory of el-ph coupling in moderately and strongly correlated materials is not yet fully developed. Indeed, there are indications that magnetism and electron correlations can significantly enhance el-ph coupling [34,35,36,37,38, 39,40,41]. For example, the cations surrounding the Fe-layers can screen the Hubbard U [38,39,40] and establishing novel lattice couplings (via modulating the screened el-el interactions [40], by changing relevant single particle quantities [41], *etc.*). Thus, there can be novel sources for the el-ph interactions that are not accounted for in traditional DFT calculations [8]. These effects might be responsible for the huge magneto-elastic coupling to the As-derived A_{1g} phonon mode in and near the regions of coexistence between magnetism and superconductivity showing in particular a large deformation potential of about (0.1 to 0.15) eV/nm in the parent compound $BaFe_2As_2$ [42], and the observation of magneto-elastic coupling for $Ba(Fe_{1-x}Co_x)_2As_2$, even at room temperature [43] (see also Refs. [44,45,36]). Several observed phonon anomalies [46,47,48] also point to significant couplings between the lattice and the charge, spin, or orbital degrees of freedom. Regarding the previously mentioned small empirical values of λ_{e-ph} derived from the high-energy relaxation rates, we remind the reader that this measurement accesses the transport coupling constant, which weights backscattering processes and differs from el-ph coupling that enters Eliashberg theory [49]. These considerations show that el-ph coupling cannot be ruled out *a priori* in moderately to strongly correlated materials based on DFT arguments alone. Indeed, some studies have inferred a significant contribution from the lattice [24,36,37,20,19].

1.2 Mass renormalizations and band shifts.

Other fundamental and still unresolved questions concern the role of retardation (frequency) and the particular momentum dependence of the interactions responsible for pairing (dominated for instance by specific nesting vectors [30] for small momentum transfers [50,20,33]). A full accounting of all of these effects in detail is practically impossible for the multi-band Fermi surfaces present in the FeSC; nevertheless, the effective mass m^* of the quasiparticles near the Fermi level of a Fermi-liquid-like system can provide some insight into the overall strength of the many-body effects and the relevant interactions. This information is encoded in the real part of the complex-valued electron self-energy $\Sigma(\mathbf{k}, \omega) = \Sigma'(\mathbf{k}, \omega) + i\Sigma''(\mathbf{k}, \omega)$,

$$\frac{m^*(\mathbf{k}_F)}{m_b(\mathbf{k}_F)} = \frac{1 - \partial \Sigma'(\omega, T, \mathbf{k}_F) / \partial \omega}{1 - \frac{\partial \Sigma'(\omega, T, \mathbf{k}_F)}{\partial \mathbf{k}}}, \quad (2)$$

where m_b is the bare mass in the absence of interactions and ω is the quasiparticle energy measured relative to the Fermi level.¹

For our purpose, we will take m_b as the band mass computed by DFT calculations, where the correlation effects introduced by the various DFT exchange-correlation potentials (Slater, Perdew, *etc.*) are small. In doing so, the ratio m^*/m_b then gives an approximate measure of the strength of the interactions beyond the single-particle picture provided by DFT.

As mentioned, the electronic interactions in the FeSCs provide a contribution to the total mass enhancement at the Fermi level. However, they are also believed to be responsible for the exchange bosons that act as the pairing mediator in these materials. According to most scenarios, the exchange bosons are restricted to a low energy interval of approximately 0 – 300 meV, considerably below the typical energy scale of the Hubbard $U \sim 2 - 4$ eV or Hund's exchange $J \sim U/4$ [51]. Thus, in these frameworks, the pairing interaction represents only a fraction of all interactions present in the system. Similarly, the el-b interaction must also provide only a portion of the total mass m^* or the relative energy shifts of the various bands. [Formally, one can extend such bosonic descriptions to higher energies [52, 53] using flexible model expressions for the self-energy entering Eq. (2), and such approaches have been applied successfully to Sr_2RuO_4 and other $4d$ systems.] Based on this, we suppose that the total coupling λ can be partitioned into “high”- and “low”-energy contributions, where the typical energies differ at least by an order of magnitude. Here, we regard the high-energy part as encompassing energies ranging from about 500 meV to the bandwidth, while energies $\leq 200 - 500$ meV represent the residual bosonic excitations entering the kernels of the Eliashberg equations. The latter in principle contains the action of the phonons as well as any spin and charge fluctuations established by the electronic interactions. (Note that this is an approximate partition. In the vicinity of an orbital-selective Mott transition, the Hund's rule coupling J can also be active at low energies and high temperatures through its role in determining the “bad metal” incoherence regime.)

With this partition in mind, it is convenient to rewrite Eq. (2) in an approximate factorized form, which separates the contributions from the two energy regimes

$$\begin{aligned} \frac{m^*}{m_b} &= (1 + \lambda) \\ &\approx \left(1 + \lambda_{el-el}^{high}\right) \left(1 + \lambda_{el-b}^{low}(T)\right) \\ &\approx \frac{m_{high}^*}{m_b} \left(1 + \lambda_{el-b}^{low}(T)\right). \end{aligned} \quad (3)$$

¹ The self-energy can also result in significant shifts of the individual bands, which can dramatically change the effective mass in cases where empty bands are near the Fermi level, or in the presence of shifted van Hove singularities. These effects can be necessary for the understanding both the normal and superconducting states of the FeSCs and are discussed in Sec. 3.2.

Here, λ denotes the *total* coupling strength including the effects of all interactions, $\lambda_{\text{el-el}}^{\text{high}}$ is the Fermi-surface averaged contribution of the el-el interactions at high-energies and $\lambda_{\text{el-b}}^{\text{low}}(T)$ is the low-energy contribution (renormalized by the pre-factor [53]) from the various retarded interactions mediated by exchange bosons. (For brevity we will drop the T dependence from our notation; however, this quantity can vary with T when superconductivity is fed back into the bosonic spectrum.) The latter includes the bosons acting as the superconducting glue and potentially others that do not contribute to pairing but still dress the quasiparticles. For instance, in d -wave superconductors the latter might include bosons with a momentum-independent coupling, which will contribute the effective mass while providing no contribution to d -wave pairing [54,55].

1.3 Quantifying the high-energy renormalization.

A rough estimate of the high-energy contribution to the mass renormalization can be obtained by comparing measurements of quantities such as the total electronic bandwidth or plasma frequency against the predictions of DFT. For example, the value of $1 + \lambda_{\text{el-el}}^{\text{high}}$ should be approximately equal to the ratio of the overall measured and DFT-calculated electronic bandwidths. Similarly, ignoring some uncertainties related to impurity scattering, one can get a similar estimate by comparing the squares of the calculated total intraband plasma frequency $\Omega_p^2 = \sum_i \Omega_{p,i}^2$, where i is a band index, to the experimental values for Ω_p^2 at room temperature.

We have carried out such an exercise for several of the FeSCs using the total plasma frequencies, and compare the experimental plasma frequencies to the values obtained from our DFT calculations in Tbl. 1. For La-1111 or Ba-122 we find a value of $1 + \lambda_{\text{el-el}}^{\text{high}} \sim 2.78$, while for the more correlated K-122 we find $1 + \lambda_{\text{el-el}}^{\text{high}} \sim 6$.

Before proceeding, we note that in the case of CaFe_2As_2 we have adjusted the values of Ω_p from the ones reported in Ref. [57]. Typically one obtains the plasma frequency in the FeSCs by fitting optical conductivity data with at least *two* Drude peaks for the sake of simplicity. In doing so, one usually finds (see e.g. Ref. [59]) that one of the Drude peaks is quite broad compared to the other. This also happens in the two special cases under consideration Ca-122 and K-122 [57,60,61,62]. This simple and minimal fitting procedure, which is at first glance reasonable, might yield misleading results, however. This possibility is evident in the fact that it sometimes results in Ω_p values that are comparable to or exceed the calculated DFT values, leaving no room for additional renormalizations by interactions. For example, Ref. [57] reported a $\Omega_{p,2} = 20500 \text{ cm}^{-1}$ (2.54 eV), which nearly coincides with our calculated total Ω_p , and yields in turn a small mass renormalization and a large scattering rate corresponding to a mean free path $l < 10 \text{ nm}$. In our opinion, the solution to this puzzle is to decompose the unusually broad Drude peak into two sub-components: a narrower Drude peak with a smaller partial

| Compound | Ω_p (DFT) | Ω_p (Exp.) | $\frac{m^*_{\text{high}}}{m_b}$ | |
|----------------------------------------------------------------------|------------------|-------------------|---------------------------------|---|
| LaOFeAs | 2.2 | 1.33 | 2.7 ± 0.1 | P |
| LaO _{0.9} F _{0.1} FeAs | 2.2 | 1.37 | 2.33 | P |
| LaO _{0.9} F _{0.1} FeAs _{0.9} | | ≤ 1.3 | | P |
| SrFe ₂ As ₂ | 2.8 | 1.72 | 2.63 | S |
| La _x Sr _{1-x} Fe ₂ As ₂ | 2.8 | | | |
| SrFe _{2-x} Co _x As ₂ | 2.7 | | | |
| BaFe ₂ As ₂ | 2.63 | 1.66 | 2.51 | S |
| BaFe ₂ As ₂ | | 1.58 | 2.78 | S |
| K _x Ba _{1-x} Fe ₂ As ₂ | 2.63 | 1.6 | 2.78 | S |
| K _{0.45} Ba _{0.55} Fe ₂ As ₂ | 2.63 | 1.7 | 2.39 | S |
| CaFe ₂ As ₂ | 2.95 | 1.85 | 2.56 | S |
| CaFe ₂ As ₂ | 2.95 | 2.71 | 1.19 | S |
| CaFe ₂ As ₂ | 2.95 | 2.33 | 1.6 | S |
| LiFeAs | 2.9 | 1.93 | 2.27 | S |
| KFe ₂ As ₂ | 2.54 | 1.04 | 6.0 | S |

Table 1 Calculated (DFT) and experimental unscreened in-plane plasma frequencies (\parallel ab) in units of eV. We used the virtual crystal approximation for the calculations of the doped systems. P and S stand for polycrystalline sample and single crystal, respectively. The experimental data are taken from Ref. [56] for LiFeAs, Ref. [57] for CaFe_2As_2 . For the other compounds see, Ref. [58]. Here, m_b is obtained from DFT calculations.

Ω_p and an additional interband transition at relatively low energies.

We believe that this is a general phenomenon in the FeSCs, where the broad Drude peak frequently obtained from optics data likely contains a contribution from a low-lying interband transition (probably below the first Lorentz peak at about 6000 cm^{-1} [0.75 eV]). This interband transition is typically unresolved due to the nearly structureless optical spectra below 1.2 eV (shown for example in Fig. 5b of Ref. [57]). This hypothesis is supported by reports of such interband transitions in measurements for Ba-122 [63,64] and in DFT calculations [65]. It can further be corroborated using an alternative measure of Ω_p obtained by integrating the real part of the dielectric function [57]. In the case of Ca-122, one would arrive at $\Omega_p \approx 1.96 \text{ eV}$ and a mass renormalization of 1.68, which is clearly still too small. But for the weakly correlated undoped Ca-122 [66], this procedure yields a more reasonable mass renormalization of 2.56 when one adopts 15000 cm^{-1} (1.86 eV) for the experimental Ω_p . This value is a bit smaller than one of the available data for Ba-122 with larger lattice constants. For the heavily hole doped $\text{Ca}_{0.32}\text{Na}_{0.68}\text{Fe}_2\text{As}_2$ [19] a markedly larger mass renormalization of 4.25 ± 0.25 is obtained using the corresponding μSR -data [67] and employing the relations given in Refs. [39,68]. For this reason, in the case of K-122 being of special interest (see Sec. 3), we replaced the experimental $\Omega_{p,2} = 20500 \text{ cm}^{-1}$ [57] by a much smaller value of $\tilde{\Omega}_{p2} = 7514 \text{ cm}^{-1}$ (0.93 eV).

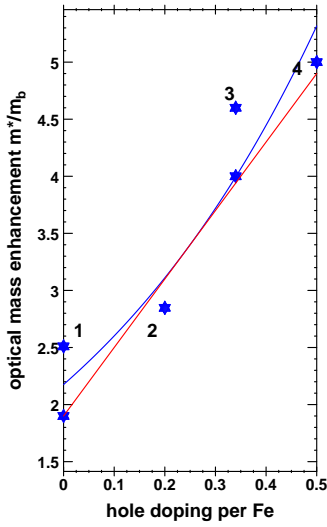


Figure 1 (color online) The empirical optical mass enhancement for various relative clean 122 FeSCs with doping outside the FeAs- layers and different hole content using the data shown in Tab. 1: Red and blue curves are linear and exponential regression based guides to the eyes, respectively. The large error bars in the optical data due to the presence of several interband transitions do not allow to resolve the expected positive curvature.

The latter exceeds the experimentally well-defined lower $\Omega_{p,1} = 6500 \text{ cm}^{-1}$ (0.81 eV) obtained for the other Drude component. As a result, we arrive at a dominant high-energy mass renormalization of about six necessary to describe its large Sommerfeld constant γ and the superconductivity mediated by weaker low-energy bosonic interactions (see below).

All of the above analysis has been carried out using the room temperature plasma frequency in the normal state. If one wishes to do a similar study in the superconducting state, then some additional care must be taken to account for the possibility that not all electrons take part in forming the superconducting condensate. For example, a crude rescaling of the zero temperature London penetration depth Λ for hole-overdoped system $\text{Ba}_{0.35}\text{Rb}_{0.65}\text{Fe}_2\text{As}_2$ [69], which is a candidate for d -wave superconductor as in Rb-122, gives

$$\frac{\Omega_p^{\text{BaRb}} \Lambda^{\text{BaRb}}(0)}{\Omega_p^{\text{CaNa}} \Lambda^{\text{CaNa}}(0)} \approx \sqrt{\frac{(1 + \lambda^{\text{BaRb}}) n^{\text{BaRb}} n_s^{\text{CaNa}}}{n_s^{\text{BaRb}} n^{\text{CaNa}} (1 + \lambda^{\text{CaNa}})}}$$

where n is the total charge density of all conduction electrons, and n_s is the part residing in the condensate at $T = 0$. Note that for an electronic or magnetic pairing mechanism, some of the electrons are components of the

pairing interaction, and therefore one expects $n_s/n < 1$.² Using the experimental London penetration depth data of $\Lambda^{\text{BaRb}} = 257 \text{ nm}$ [69] $\Lambda^{\text{BaRb}} = 194 \text{ nm}$ [67], $\lambda^{\text{CaNa}} = 0.89$ [19], and adopting a comparable total coupling constant $\lambda^{\text{BaRb}} \approx 1$ and similar unscreened plasma frequencies, we estimate $n_s^{\text{BaRb}} \approx 0.6$, only. This way by quenching the weakly coupled d_{xy} -derived band by the combined effect of a weak magnetic field and disorder, the single-gap d -wave scenario might be in principle understood.

We have performed a similar phenomenological analysis of different optical conductivity and penetration depth measurements for several FeSCs as a function of hole doping. The results, summarized in Fig. 1, reveal a steep increase of the mass renormalization with hole doping, in qualitative agreement with the Hund's metal picture proposed by the DMFT [70] and the slave-boson approximations [71]. Similar constraints on the value of $\lambda_{\text{el-el}}^{\text{high}}$ can be placed on other compounds. For example, an orbital-resolved ARPES analysis for the undoped LiFeAs and the el-doped $\text{Ba}(\text{Fe}_{0.92}\text{Co}_{0.08})_2\text{As}_2$ results in comparable numbers for the band renormalization renormalization: about 2.3 and 2.1 for the el-pockets with $3d_{xz}/d_{yz}$ and $3d_{xy}$ character in Ba-122 and 2.2 (1.8) for the el (h)-pockets with $3d_{xz}/d_{yz}$ character, but 4 (3.3) for the el (h)-pockets of $3d_{xy}$ character in LiFeAs . The increased values of the former are in accord with the DMFT predictions for the importance of correlation effects for the $3d_{xy}$ states with further h-doping. [72, 73, 74, 75].

2 Weak versus strong coupling in Fe-based superconductors. Having obtained rough estimates for the high-energy contribution to the mass renormalization, we now turn our attention to the low-energy contribution coming from el-b interactions.

The single-band BCS model describes many weak-coupling superconductors. This model predicts universal thermodynamic relations in the weak coupling limit. While this is consistent with measurements on weakly coupled conventional superconductors, notable deviations occur in strongly-coupled cases. Strong-coupling Eliashberg theory can account for these discrepancies by taking into account the retarded nature of the effective attractive interaction mediated by phonons [76]. Based on this success, many have attempted to generalize this approach to unconventional superconductors, which are believed to be strongly coupled due to their large values of T_c . In the case of the FeSCs, such schemes must also be generalized further to include multiband effects. Implicit in this approach is the assumption that boson-exchange frameworks are the appropriate language to describe pairing in unconventional

² This effect is usually small and was ignored in Ref. [19], were we adopted $n_s/n \approx 1$ for the optimally Na-doped Ca-122 system for the sake of simplicity. Below we will consider a much more dramatic case, where one band with a substantial DOS and a marked contribution to the total plasma frequency is quenched at low temperature.

superconductors [51, 77]. Here, we will not discuss the validity of this outlook but merely comment on the restrictions placed on it in the context of the FeSCs.

To estimate the total interaction with low-energy bosonic modes, we must examine quantities that are sensitive to the mass changes at the Fermi level. One such quantity is the Sommerfeld coefficient γ , which characterizes the linear in T contribution to the electronic specific heat. For an interacting system γ is written as

$$\gamma = (1 + \lambda) \gamma_b, \quad \gamma_b = \frac{2}{3} \pi^2 k_B^2 N_b(0), \quad (4)$$

where γ_b is the “bare” Sommerfeld coefficient for the non-interacting system, k_B is the Boltzmann constant, $N_b(0)$ is the bare DOS at the Fermi level (taken from band structure calculations), and λ is the *total* band-averaged coupling constant due to all interactions. Therefore, if one knows γ and $\lambda_{\text{el-b}}^{\text{high}}$, one can estimate $\lambda_{\text{el-b}}^{\text{low}}$.

The values of the average and band-resolved coupling constants at low-energy $\lambda_{\text{el-b}}^{\text{low}}$ in the FeSCs are still under debate, and several Eliashberg-based studies arrive at different values for the total coupling. Shortly after the discovery of FeSC, $\text{LaFeAsF}_{0.1}\text{O}_{0.9}$ was identified as being in an *intermediate* coupling regime with $\lambda_{\text{el-b}}^{\text{low}} = 0.61 \pm 0.35 < 1$ [68, 39, 58]. This estimate was obtained using the well-known mass dependence of the superconducting condensate density determined by the low-temperature penetration depth measurements. Similarly, the upper critical field $H_{c2}(T)$ for a sample with strong paramagnetic effects due to the presence of As vacancies were also successfully described using the same weak to intermediate coupling regime [78, 79]. In contrast, a $\lambda_{\text{el-b}}^{\text{low}} \sim 2$ was obtained for optimally doped $\text{Ba}_{1-x}\text{K}_x\text{Fe}_2\text{As}_2$ ($T_c = 38$ K) [80, 81] from specific heat and optical data within a four-band Eliashberg model. This result is larger than the $\lambda_{\text{el-b}}^{\text{low}} < 1.5$ estimated by L. Benfatto *et al.* [22] for the same compound also within a four-band model.

We recently performed similar calculations for the specific heat of $\text{Ca}_{0.32}\text{Na}_{0.68}\text{Fe}_2\text{As}_2$ ($T_c = 34.4$ K) using a three-band model. Figure 2 reproduces the main results. By fitting the data we arrived at $\lambda_{\text{el-b}} = 0.88$ [19]. The three-band description allowed us to decompose the involved coupling constants, which included a dominant pair of bands coupled by a significant repulsive interband coupling with $\lambda_{12} = -1$ and a weakly coupled third band with $\lambda_{13} = -0.1$ and $\lambda_{23} = 0$. Surprisingly, we also obtained a non-negligible attractive intraband interaction (interpreted as due to el-ph coupling or perhaps orbital fluctuations) $\lambda_{11} = \lambda_{22} = \lambda_{33} = 0.45$ (taken to be equal in this case to reduce the number of fitting parameters). This value is twice as large as the typical DFT based estimates [8] but was needed to reproduce the pronounced knee observed in the specific heat at $T/T_c \sim 0.3$. In this model, the repulsive interband interaction still provides the majority of the total T_c : switching off the el-ph interaction, we obtained a relatively high $T_c = 21.7$ K, but switching off the spin-fluctuations produced $T_c = 5.4$ K.

Our model for $\text{Ca}_{0.32}\text{Na}_{0.68}\text{Fe}_2\text{As}_2$ predicted $T = 0$ gap values of $\Delta_1 = 7.48$ meV, $\Delta_2 = 2.35$ meV, and $\Delta_3 = 7.5$ meV, in agreement with ARPES [82] ($\Delta_1 \approx \Delta_3 = 7.8$ meV and $\Delta_2 = 7.48$ meV) and μSR (6 – 6.7 meV and 0.6 – 0.8 meV within a finite magnetic field) measurements. Another ARPES study [83] arrived at somewhat larger gaps [83] for a single crystal with the same T_c (see Tab. 2). Experimentally, the smallest gap occurs on the outermost hole Fermi surface with d_{xy} -character.

Several independent analyses have arrived at similar estimates for $\lambda_{\text{el-b}}^{\text{low}}$. For example, a recent analysis of optical data for nearly optimally doped $\text{Ba}_{0.6}\text{K}_{0.4}\text{Fe}_2\text{As}_2$ ($T_c = 39$ K) and LiFeAs ($T_c = 17$ K) by J. Hwang [84] extracted the el-boson spectral densities (the Eliashberg function) within an effective single band approach. The measured total plasma frequencies of the superconducting condensate $\Omega_c^2 \approx \Omega_{\text{unscreened}}^2 / (1 + \lambda_{\text{el-b}}^{\text{low}})$ are 1.01 eV for $\text{Ba}_{0.6}\text{K}_{0.4}\text{Fe}_2\text{As}_2$ and 0.87 eV for LiFeAs . In the clean limit, this yields $\lambda_{\text{el-b}}^{\text{low}} = 1.51$ for the former (if the empirical value of $\Omega_{\text{unscreened}} = 1.6$ eV [80] is used instead of the *adopted* 1.8 eV and claimed $\lambda_{\text{el-b}}^{\text{low}} = 1.98$ by the author). This value is in perfect agreement with our estimate based on the Sommerfeld constant γ and a high-energy

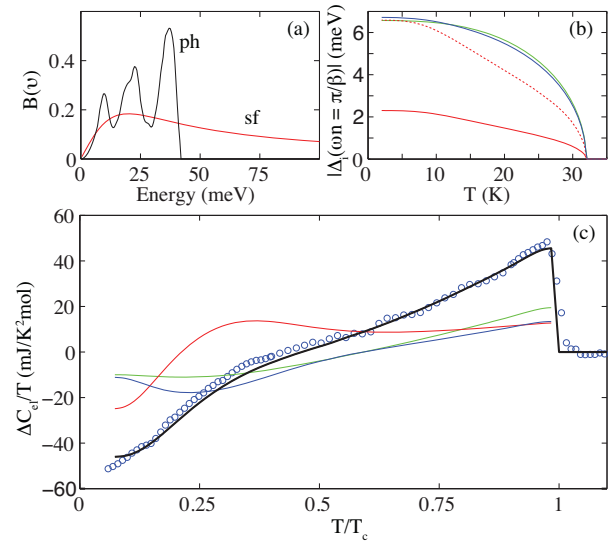


Figure 2 (color online) Adopted Eliashberg-functions (a), calculated gaps (b) and the fitted electronic specific heat (c) employed for the theoretical description of optimally Na-doped Ca-122 (see text) as described within an effective three-band model, taken from Ref. [19]. Notice the hump at about $0.35T_c$ which stems from the phenomenologically large PDOS of the weakly coupled third band with dominant Fe $3d_{xy}$ character reflecting this way the high-energy mass renormalization. A similar feature is observed at weak interband coupling for the weakly coupled β -band in $\text{K}(\text{Rb},\text{Cs})\text{-122}$ (see Sect. 5)

renormalization of 2.5 inferred from the ARPES data [85]. This value also agrees well with the four-band analysis by L. Benfatto *et al.* [22], and is also closer to 0.9 obtained for optimally Na-doped Ca-122 [19]. Thus, three independent analysis arrive at an intermediate coupling regime for FeSCs with $T_c \leq 40$ K. A weak coupling regime is also implied for LiFeAs. Using the recent optical data for LiFeAs [56] (see also Tab. I) with $\Omega_{\text{unscreened}} = 1.93$ eV. Similarly, several analyses for LiFeAs have arrived at small values for $\lambda_{\text{el-b}}^{\text{low}}$. For example, an analysis of specific heat similar to that shown in Fig. 2 [86] arrives at $\lambda_{\text{el-b}}^{\text{low}} \approx 0.6$ while comparable values of $\lambda_{\text{el-b}}^{\text{low}} \approx 0.8$ were obtained from scanning tunneling microscopy [87, 88] and 0.89 from optical data [84] (once a realistic value of the unscreened plasma frequency is adopted).

The possibility of changing the coupling regime from weak to strong across the various Fe pnictide families was proposed in Ref. [89], based on an analysis of the $2\Delta(0)/k_B T_c$ ratio, as well as the jump in the specific heat $\Delta C_v(T_c)/T_c$. According to that analysis, optimally K-doped Ba-122 is the most strongly coupled FeSC. However, given the collection of results summarized above, we believe it is clear that many FeSCs have an intermediate coupling to the low-energy bosonic modes. Furthermore, we are in a position to explain several difficulties in the $\lambda_{\text{el-b}}^{\text{low}} \sim 2$ estimated obtained for $\text{Ba}_{1-x}\text{K}_x\text{Fe}_2\text{As}_2$, which underestimates the high-energy renormalization. Using the experimental value of the Sommerfeld coefficient $\gamma \approx 50$ mJ/mol \cdot K² [90] and the DFT-calculated $\gamma_b = 9.26$ mJ/mol \cdot K² [91], we arrive at $(1 + \lambda) = \gamma/\gamma_b \approx 5.3$, which must be partitioned between the high- and low-energy interactions. The high-energy contribution can be estimated as outlined in the previous section. Ref. [85] reported significant high-energy bandwidth renormalizations of 2.94 and 1.98 for the inner and outer hole pockets at Γ , and 1.58 for the hole pocket at the

X -point. If we adopt comparable PDOS-values for each band, we estimate $1 + \lambda_{\text{el-el}}^{\text{high}} < 2.2$, which is a little lower than the values $\approx 2.4 - 2.7$ obtained from the plasma frequencies (Tlb. 1). From these estimates, we then see that $\lambda_{\text{el-b}}^{\text{low}} \sim 2$ would require a $\lambda_{\text{el-el}}^{\text{high}} \sim 1.77$, which is too small compared to any of our estimates. By comparison, $\lambda_{\text{el-b}}^{\text{low}} \leq 1.5$ allows for a $1 + \lambda_{\text{el-el}}^{\text{high}} \sim 2.2$, which is within our range.

This discrepancy likely stems from the use of the DFT-derived PDOS in Ref. [81] in place of the high-energy renormalized values (as considered in Ref. [22]). Another factor might be related to some underestimation of the strength of the el-ph (or orbital fluctuation) interaction adopted in the modeling of the multiband interaction matrix. A similar overestimation of the spin-fluctuation interaction is present in the model calculations by Ummarino *et al.* [25,26,92]. There, the low-energy bosonic coupling constants are $\lambda_{\text{el-b}}^{\text{low}} \sim 4 - 5$, which has the same fatal consequences for the Sommerfeld constant γ and the high-energy mass renormalizations. Only in their most recent paper (devoted mainly to $\text{FeTe}_{1-x}\text{Se}_x$ [24] analyzed within a three-band model), did the authors allow for a sizable intraband coupling ascribed to the el-ph interaction present in the third el-pocket, only. This way they arrive at $\lambda_{\text{el-b}}^{\text{low}} = 1.48$ and $\lambda_{\text{el-ph}}^{\text{low}} = 1.1$. The last value seems to be somewhat large, but it can be lowered by adopting a weak intraband coupling in the remaining two bands as well. It is also noteworthy that the authors demonstrated the significance of a self-consistent calculation by accounting for the feedback of superconductivity on the spin fluctuations within their approach, which is usually ignored in Eliashberg calculations.

For the remainder of this section we will discuss several subtle issues that can affect assessments of the total el-b coupling in the FeSCs. In this context, two more results of Ref. [84] are noteworthy. First, in addition to the dominant narrow peak near 15 meV expected for the interband spin fluctuations, the extracted spectral density has a second broader peak centered at ~ 48 meV. This higher-energy peak is absent in the models adopted in Refs. [22, 80,81]. Second, the analysis of the normal state optical properties at 40 K (just above T_c) shows a hardening of the first dominant peak compared with the data deep in the superconducting state ($T = 4$ K). This observation yields a $\lambda_{\text{el-b}}^{\text{low}}$ that is enhanced by about 10% as compared to the normal state. Such an empirical T -dependent boson spectrum was not accounted for in Refs. [19,22,80,81] and might have an impact on the temperature dependence of the specific heat and the zero temperature gap values. Verifying the T -dependent spectral density by other measurements is of considerable interest since it provides new insight into the interplay between magnetism and superconductivity.

Ignoring the high-energy band renormalizations can result in inaccurate estimates of the size of the of specific heat jump $\Delta C/\gamma_n T_c$ and other observables. Another

| $\Delta_i(0)$ | ARPES | ARPES | μSR | $C(T)$ |
|----------------------------------------------------------|-------|-------|----------------|--------|
| $\text{Ca}_{0.33}\text{Na}_{0.67}\text{Fe}_2\text{As}_2$ | | | | |
| Δ_1 | 10.2 | 7.8 | 6.7 ± 1.3 | 7.5 |
| Δ_2 | 5.7 | 2.3 | 0.7 ± 0.1 | 2.35 |
| Δ_3 | 9.2 | 7.8 | 6.7 ± 1.3 | 7.48 |
| $\text{Ba}_{0.33}\text{Rb}_{0.65}\text{Fe}_2\text{As}_2$ | | | | |
| Δ_1 | | | 8.4 | |
| $\text{Ba}_{0.1}\text{K}_{0.9}\text{Fe}_2\text{As}_2$ | | | | |
| Δ_1 | 3.2 | – | – | – |
| Δ_2 | 2.9 | – | – | – |
| Δ_3 | 2.7 | – | – | – |

Table 2 Experimental and theoretical values for multiband gaps in meV of two strongly hole doped 122 FeSC, Na-doped Ca-122 and Rb-doped Ba122, described in effective single, two-band and three-band models as derived from ARPES, specific heat and penetration depth (μSR) data (see text).

many-body effect that is potentially significant for multi-band systems is the possible chemical potential shifts associated with charge redistribution below T_c [93,94]. Any strong coupling regime deduced from a simple Eliashberg-theory calculation that ignores changes of the chemical potential in the superconducting state – especially for narrow or shallow bands – will miss this contribution to the jump in the specific heat and other observables. As an instructive illustration, we refer to recent work using simpler models where such chemical potential shifts were neglected [95, 96,97]. An advanced multiband Eliashberg analysis along these lines is necessary to reconsider/check the strong coupling results mentioned above.

A weak-coupling interband regime within two- and three-band descriptions has also been found for Co-doped Ba-122 [59,98], based on specific heat and optical data. These works found a non-BCS shape of the T -dependent small gap functions, which affected the behavior of the penetration depth, in contrast to a BCS-like shape expected for a dominant interband coupling. This shape clearly points to the presence of a significant intraband coupling in this el-doped system, similar to Fig. 2. It also might explain the possibility for a symmetry change of the SCOP with increasing disorder at a reduced but still significant T_c [16].

Finally, let us consider the case of strongly el-doped LaFeAsO $_{1-x}$ H $_x$ and $x = 0.2$, where a rather large $T_c = 48$ K (52 K) was reported under 3.0 GPa (6.0 GPa) of pressure [99]. The increase in T_c was observed *without* any indication corresponding to stronger spin fluctuations (which might at first glance explain the significant T_c enhancement under pressure) as deduced from both NMR and inelastic neutron scattering measurements. In such a situation a dominant conventional intraband mechanism based on phonons or orbital/charge fluctuations is very likely. A rough estimate for the corresponding coupling constant can be obtained from an approximate analytical expression for T_c (derived for an intermediately coupled effective single-band superconductor [100])

$$\lambda = \frac{1}{[\ln(\omega_{\text{ln}}/k_B T_c) - 1 - A + \ln(1.13)]}. \quad (5)$$

Adopting $\omega_{\text{ln}} \sim 35 - 40$ meV, as suggested by couplings to As-phonons, and a shape factor $A \approx 0.5$ valid for a narrow peak in the Eliashberg function, one arrives again at $\lambda_{\text{el-b}}^{\text{low}} = 1.32$ (1.48) for $\omega_{\text{ln}} = 35$ meV and $\lambda_{\text{el-b}}^{\text{low}} = 1.12$ (1.23) for $\omega_{\text{ln}} = 40$, respectively. Both sets of values are again in an intermediate coupling regime. Based on this, a $T_c = 52$ K might be readily achieved e.g. by adding a weak coupling to residual interband spin fluctuations, or with crystal field excitations (CFE) specific for rare earth systems. The latter can be either attractive or repulsive [101]. Note that such a weak coupling with conduction electrons at 3 meV has been observed in the anti-ferromagnetic superconductor HoNi $_2$ B $_2$ C in point contact measurements [102]. In undoped NdFeAsO, correspond-

ing peaks at 7.2 meV and 8.6 meV have been observed [103] by inelastic neutron scattering. In LaFeAsO $_{1-x}$ H $_x$, both CFE cases might be helpful to enhance T_c , depending on the symmetry of the SCOP and the nature of the CFE. A more sophisticated theoretical study to unravel their dominant intra- or interband character, as well as low-energy inelastic neutron measurements, are desirable to settle this issue. Such studies would also be relevant for the various rare earth-1111 FeSC with the highest bulk T_c values apart from FeSe ultrathin films on SrTiO $_3$ substrates [104], where a high-energy oxygen derived optical phonons of the substrate may play an important role [50, 105, 106, 107, 108].

There are also general arguments against any super-strong coupling regime formally allowed within Eliashberg-theory: namely, an instability of the corresponding para-phase against lattice or magnetic polarons or other instabilities, which are beyond standard Eliashberg theory. In the vicinity of structural transitions, anharmonicity might also be significant and can result in temperature dependent spectral densities and anomalous isotope coefficients [109, 110, 111]. Notice that the highest coupling observed to date in a confirmed phonon-mediated superconductor ($\lambda_{\text{el-ph}} \leq 2.9$) occurs in amorphous PbBi-based superconductors [112, 113]. A lattice instability might be thwarted there by additional barriers stabilizing the metastable glassy state. In this general context, the recent observation of strong Fe-As bond fluctuations in a double-well potential by EXAFS measurements on undoped and superconducting LaFe $_{1-x}$ Co $_x$ AsO single crystals [114] is of interest. There, T -dependent tunneling frequencies at about 24.6 and 26.7 meV (6 and 6.5 THz) were reported at low-temperature. Linking these observations to novel intraband couplings or polaronic effects in the H-doped La-1111 systems will require more sophisticated theoretical tools and comparable experimental data.

To summarize this section, we believe that no FeSCs realizes a low-energy bosonic coupling regime with $\lambda_{\text{el-b}}^{\text{low}} > 1.5$, with the possible exception of the rare earth 1111 high- T_c (~ 50 K) compounds. To the best of our knowledge, no high-quality specific heat data are available for this system due to the small size of the available single crystals. But even in this case, an intermediate coupling scenario cannot be excluded at this time.

3 AFe $_2$ As $_2$, A = K, Rb, Cs puzzles - a challenge for theory. The AFe $_2$ As $_2$ families with A = K, Rb, Cs form a special group among the FeSCs. They all have rather low T_c values of only few Kelvin, which decreases in moving from K- to Cs-122 [115]. The small and decreasing T_c is attributed to an increasing proximity to a QCP, where fluctuations produce a mass enhancement but no compensation by the pairing interaction.

The phase related to the QCP has not been identified yet, but it is unlikely to be related to a Mott phase. K-122, Rb-122, and Cs-122 are the most heavily h-doped

Fe-pnictides, formally achieving a $\text{Fe}^{+2.5}$ valence state, midway between Fe^{+2} and Fe^{+3} . The former occurs in the magnetic parent compounds Ba(Sr,Ca)-122, whereas the latter is expected to form an antiferromagnetic Mott-insulator. Generally speaking, the Fe^{2+} valence state should be less correlated than the Fe^{3+} , but both should realize *commensurate* magnetic phases. Instead, one observes soft *incommensurate* magnetic fluctuations in K-122 at $T = 12$ K, where it appears as a broad peak in the spin susceptibility centered at ~ 8 meV [116]. (This energy scale is significantly lower than the resonance mode energy employed in most of the strong coupling simulations mentioned above [25,81].) BaMn_2As_2 and LaMnAsO have five electrons in their $3d$ -shells [117] and are therefore expected to be in the vicinity of a Mott-insulator phase. These systems have very high Neél temperatures of $T_N = 625$ K and 350 K, respectively. This is in sharp contrast with the three compounds discussed here, so it is unlikely that these materials are in the vicinity of a Mott phase. Therefore another magnetic phase should be considered as a candidate responsible for the QCP.

We would like to stress that the central theoretical problem in our opinion is not whether there are strongly correlated electrons (likely the $3d_{xy}$ states) present in these compounds. The Curie-Weiss tails of the measured magnetic susceptibilities at high temperatures $T > T^*$ already evidences this fact [118]. Instead, more subtle questions must be addressed, namely which of the subsystems is responsible for the QCP, which determine the nature of the magnetic phase beyond, and which form the bands where superconductivity occurs? And, how strong are the correlation effects in the corresponding subsystems? Thus K-, Rb-, and Cs-122, confront us with a complex multicomponent problem that has not been examined in detail from a theoretical point of view.

To provide a clear starting point for a discussion of related aspects given below, we performed various high-precision density functional theory (DFT) calculations for the densities of states (DOS), as well as the Fermi surface sheets including a wave vector and orbital-resolved analysis of the mass anisotropies. Our relativistic DFT electronic structure calculations were performed using the full-potential FPLO code [119,120]. For the exchange-correlation potential, both the local density approximation (LDA) within the parametrization of Perdew-Wang [?] or the general gradient approximation (GGA) with the parametrization of Perdew-Burke-Ernzerhof [121] have been chosen. The spin-orbit (SO) coupling was treated non-perturbatively by solving the four component Kohn-Sham-Dirac equation [122]. The final calculations were carried out on a well-converged mesh of maximal 10^6 k -points ($100 \times 100 \times 100$ mesh, but at least a $72 \times 72 \times 72$ mesh was used) to obtain correct band structure and Fermi surface information. For all calculations we used the experimental crystal structures.

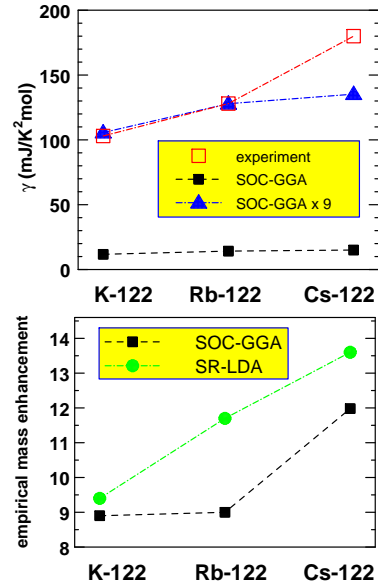


Figure 3 (color online) (a) Bare Sommerfeld constant in ($\text{mJ}/\text{K}^2 \text{ mole}$) according to our GGA calculation with SOC fully included as compared with experimental data for KFe_2As_2 (K), RbFe_2As_2 (Rb), and CsFe_2As_2 (Cs). (b) The same for the empirical mass enhancement obtained using scalar relativistic (SR) LDA and SOC-GGA calculations for total density of states (DOS) $N(0)$ at the Fermi level as reference quantity. The lines are guides for the eyes. For the experimental γ -values please see e.g. Refs. [123, 11, 105, 124] and the main text.

The K-, Rb-, and Cs-122 systems exhibit the largest Sommerfeld coefficients γ among the FeSCs, being comparable with those found for heavy-fermion systems (see Fig. 3a). This observation, together with a claimed universal Knight-shift scaling anomaly in the NMR spin-lattice relaxation rate $1/T_1 \propto T^{0.75}$ at $T < T^*$ [118] (with $T^* = 165, 125, \text{ and } 85$ K for K-, Rb-, and Cs-122, respectively), has led to proposals for a related emergent Kondo-lattice like scenario for the whole series [118]. But if one uses the DFT calculated DOS $N(0) = 5.0$ states/eV/f.u. (taking into account the SOC) and a measured Sommerfeld coefficient $\gamma \approx 103 \text{ mJ}/\text{K}^2 \cdot \text{mol}$ for KFe_2As_2 , one arrives at a large total mass renormalization of $1 + \lambda = 8.9$. This value is very close to that of RbFe_2As_2 : 8.8 (9.0), which is obtained using the experimental values of $\gamma = 125(128) \text{ mJ}/\text{K}^2 \cdot \text{mol}$ and the calculated $N(0) = 6.04$ states/eV/f.u.. In other words, these materials have almost equal mass renormalizations within the experimental error bars. This contradicts the notion that the mass enhancement increases continuously along the series from K- to Cs-122 as reported in Refs. [11, 115] (see Fig. 3b).

Our SOC GGA calculations yield the closest distance between the Fe $3d_{xz}$ - and $3d_{yz}$ -derived Van Hove singularities (VHS) and the Fermi level, as well as the largest DOS $N(0)$ at E_F as compared to LDA. Therefore, our analysis will focus on the SOC-GGA calculations to obtain conservative estimates for the corresponding renormalizations. Then, only CsFe₂As₂ with $\gamma \approx 180$ mJ/K² · mol and $N(0) = 6.4$ states/eV/f.u. shows a surprisingly increased mass renormalization $1 + \lambda = 11.98$, which is less dramatic than suggested in Refs. [11, 115, 125]. (In Ref. [125] for example, a mass renormalization of about 13 was reported for Cs-122 using the GGA-PBE within the WIEN2k package.) Note that in both of our GGA-calculations (scalar relativistic and with SOC included) we observe an almost twice as large increase of the bare DOS (28 %) in going from K-122 to Cs-122 as compared with 15% reported in Ref. [125] and 21% relative to Rb-122. We ascribed these discrepancies to our use of an unusually dense mesh of k-points ($N_{\mathbf{k}} = 72 \times 72 \times 72$) in the irreducible BZ. Note, that both LDA calculations produce a significantly smaller value of $N(0)$ (see Fig. 6). In fact, using our LDA codes, we would arrive at a somewhat larger and smoother increase in the mass renormalization in going from K-122, Rb-122, and Cs-122: $1 + \lambda = 9.4, 11.7$ and 13.6 , respectively (Fig. 3b).

An inspection of our calculated in-plane and out-of-plane plasma frequencies shows that the electronic structure according to the GGA-codes is slightly less anisotropic than those obtained within the LDA-codes. Within our approach, the SOC increases the hybridization of the electrons at the ε -Fermi surface with that on the stronger correlated β -Fermi surface. Then the SOC might also contribute to the position of the VHS, and the SOC-GGA provides the closest distance to E_F . Thus, a weaker “high-energy” el-el interaction is needed to explain the closer observed positions of the VHS (on the order of 10 meV, only). We will discuss this issue elsewhere in the context of new ARPES data.

In addition to the total mass renormalization, there are significant unexpected differences between these three compounds, even when they have similar doping levels and lattice structures. With respect to superconductivity, the symmetry of the nodal order parameter (d -wave vs. s -wave with accidental nodes) is still under debate [10, 11, 12, 128, 129, 130, 131, 132]. It is still unclear which of the five Fermi surface sheets plays a dominant role in the superconductivity and which of them are of minor relevance. Our DFT calculations of the in- and out-of-plane partial plasma frequencies find that each of the Fermi surface sheets has a distinct mass anisotropy. This result is consistent with an analysis of the T -dependence of the upper critical field anisotropy $\Gamma_H = H_{c2}^{ab}/H_{c2}^c$. Taking into account the ideal $\cos^2\Theta$ angular dependence at low-temperature [126] (see Fig. 4)

$$H_{c2}(\Theta, \mu) = \frac{\Gamma_H H_{c2,ab}^{orb}}{\sqrt{\Gamma_H^2 (\cos^2 \Theta + 2.4\mu^2(T)) + \sin^2 \Theta}}, \quad (6)$$

one finds an unexpected simple angular dependence for a multiband superconductor with rather different mass anisotropies of each of its Fermi surface sheets. For the sake of simplicity a vanishing pair-breaking for $\Theta = 0$ has been adopted in our analysis by Eq. (6), in accord with the experimental data [126, 127, 124] within the errorbars. Here, Θ measures the tilting of the external field direction from the c -axis and $H_{c2,ab}^{orb}$ is the orbital limited upper critical field without paramagnetic effects and $\mu(T)$ denotes the pair-breaking parameter (notice that $\mu(0) = \alpha_M/1.76$, where α_M is the frequently used Maki parameter) scaled by the d -wave gap function $\Delta(T)$ and the orbital limited (WHH) upper critical field [133]

$$\mu(T) = \mu(0) \frac{\Delta(T) H_{c2}^{orb}(T)}{\Delta(0) H_{c2}^{orb}(0)}. \quad (7)$$

At variance with the numerical investigation of Sr₂RuO₄ performed in Ref. [133] (which is also a multiband superconductor with a single dominant band), we have used high-quality analytical approximations for the latter two functions. From the observation shown in Fig. 4, we may conclude that only a single Fermi surface sheet survives at low T and high magnetic fields. We may identify this sheet with the blade- (propeller)-like Fermi surface (usually denoted as ε -Fermi surface sheet in dHvA-measurements) near the corner of the Brillouin zone (see Fig. 8). Thus, we suggest that this sheet of the Fermi surface is the main locus of superconductivity in K(Rb,Cs)-122, in accord with Refs. [10, 11]. But in sharp contrast, this band exhibits

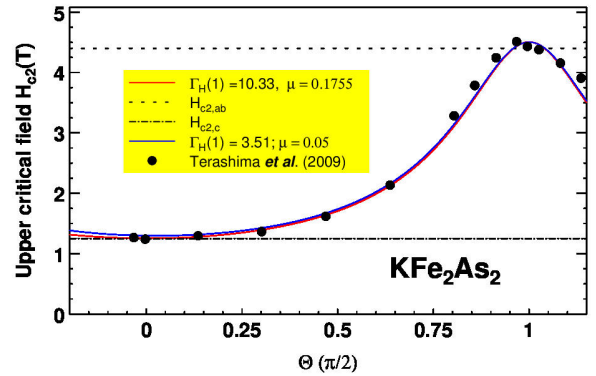


Figure 4 (color online) The anisotropy of the upper critical field $H_{c2}(\Theta)$ at low- T taken from Ref. [126], where Θ denotes the tilting angle of the magnetic field relative to the c -axis. The red line is the fit using our semi-analytic theory with an orbital mass anisotropy suggested by the calculated mass anisotropy of the ε (blade) Fermi surface sheet (see Fig. 14) and μ is the fitted pair-breaking parameter using the experimental $H_{c2}(T)$ data for $H \parallel$ to the ab -plane by F. Eilers [127] at intermediate and low- T except a small region below T_c where the four weakly coupled Fermi surfaces still participate in the superconductivity.

a nodal $d_{x^2-y^2}$ -superconducting gap in our opinion [134, 16]. In the minor remaining bands in an ambient field, however, a weak superconducting order parameter is induced which is, sensitive to competing *nonsuperconducting* order parameters. As a result, the inner Fermi surface sheet might be fully gapped in the case of coexistence. Or, in the case of non-coexistence realized on the second Fermi surface sheet, it occurs in the four nodal regions of the d -wave superconducting order parameter, leading to an octet nodal structure in accord with high-precision laser ARPES measurements [131, 132]. Unfortunately, these same experiments cannot probe the ε -Fermi surface sheet and hence its gap structure. Further experimental and theoretical studies are necessary to settle this subtle puzzle.

The quenching of the minor bands is probably related to the non-BCS shapes of $\Delta(T)$ for these bands, which is generic for weak interband coupling. Then the significantly suppressed gap amplitudes near T_c and the enhanced magnetic susceptibility of the most correlated β -band may dramatically enhance the paramagnetic effect provided by the Zeeman-splitting [79]. This view would explain why the most anisotropic band quenches first and Γ_H is reduced already in the very vicinity of T_c . The calculated moderate mass anisotropy of the blade ε -band is in accord with the significant k_z dependence of the extremal cross sections observed in de Haas-van Alphen (dHvA) measurements reported by Yoshida *et al.* [135] (1.29 % including the Z-point and 0.89 % including the Γ -point of the BZ in units of its total area). The significant deviation of the absolute values in the DFT calculations by a factor of 10 reflect the band shifts discussed below in the context of the positions of van Hove singularities.

3.1 An unusual low-energy bosonic excitations in K-122. Recent work involving some of the current authors observed a clear bosonic peak near 20 meV in several ballistic point-contact measurements of K-122 [136]. The standard interpretation for this peak as being due to spin fluctuations or harmonic phonons can be ruled out. Our calculation of the harmonic el-ph Eliashberg function $\alpha^2F(\nu)$ revealed no sharp peak structures at this energy. Regarding spin fluctuations, the available inelastic neutron scattering data [116] shows a broad peak structure in the spin susceptibility, but at a lower energy ~ 8 meV. We are therefore forced to consider other candidates

One possibility initially advanced in Ref. [136], is that the 20 meV boson is a related to low-lying exciton, involving an electron transfer from one nested Γ -centered hole-like band to an empty electronlike band located slightly above the Fermi energy and centered near the BZ corner. This electron band is generic to all FeSCs and it becomes completely unoccupied with hole-doping at a corresponding Lifshitz-transition, which occurs at $x \approx 0.7 - 0.8$ in $\text{Ba}(\text{Sr})_{1-x}\text{K}_x\text{Fe}_2\text{As}_2$. Our DFT calculations place this band about 10 to 25 meV above the Fermi level and further show that its band minimum produces a weak van Hove

singularity (VHS) in the PDOS, as shown in Fig. 5. Here, calculations must be carried out on sufficiently dense \mathbf{k} -grids to resolve it, e.g. $N_{\mathbf{k}} = 72 \times 72 \times 72 = 72^3$ \mathbf{k} -points in the irreducible part of the BZ. This is illustrated in Fig. 5, where we show DOS results for K-122 as a function of $N_{\mathbf{k}}$. In the present case, at least $N_{\mathbf{k}} = 50^3$ are needed to achieve the necessary convergence. Usually, we have used $N_{\mathbf{k}} = 72^3$ and checked that $N_{\mathbf{k}} > 100^3$ gives practically the same result, as shown in Fig. 5. In addition to the visible impact on the sharpness of the VHS, we find that the \mathbf{k} -grid density also affects the value of the DOS at the Fermi level and deviations of up to 20 % of the converged value can be obtained for less dense grids. To the best of our knowledge, this significant \mathbf{k} -grid dependence has not been taken into account explicitly when estimating the strength of many-body effects in the pnictide literature although it is well-known in principle. Like the \mathbf{k} -mesh, the details of the lattice structure such as the As position have a significant impact on the physical properties. Generally, low- T structural data are used (if available) to analyze e.g. the Sommerfeld constant γ_b correctly. If one uses room temperature data with enlarged lattice constants to compute γ_b , which is then compared to low- T measurements, then the correlation effects can be overestimated. In the case of A-122 (A = K, Rb, and Cs), low- T structural data (down to $T = 1.7$ K) are only available for K-122 [137]. To circumvent this problem for Rb-122 and Cs-122, we scaled the available room temperature data for the latter [127] in a similar way as in K-122.

We suggest that this VHS could affect some physical properties in the vicinity of the Lifshitz transition at $x \sim 0.7 - 0.8$. The observation of an exciton is somewhat unusual for an ordinary metal since the Coulomb interaction between the excited electron, and the remaining hole is usually entirely screened. As a result, the exciton becomes ill-defined as a quasi-bosonic excitation interacting with the other conduction electrons. The heavy masses for these three systems under consideration here, however, may be helpful for stabilization of such excitons through a reduction of dynamical screening.

Alternatively, the 20 meV boson may be related to other types of excitations. In the context of charge excitations, two recent studies devoted to K-122 [138] and Rb-122 [139] are of interest. In Ref. [138] critical spin *and* charge fluctuations have been reported using pressure measurements. In Ref. [139] a partial charge order below 20 K was ascribed to an electronically driven phase separation, which is accompanied by a small gap of 17 K in the spin-lattice relaxation rate $1/T_1$ probed by NQR measurements. Alternatively, the possibility of orbital excitations or low-lying plasmon excitations (due to the presence of both very heavy and lighter electrons) should be investigated theoretically.

Another option is the vicinity of a QCP of a novel SDW phase with magnetic stripes (discussed in the next section) or strong anharmonicity of the Fe-As bond phonons

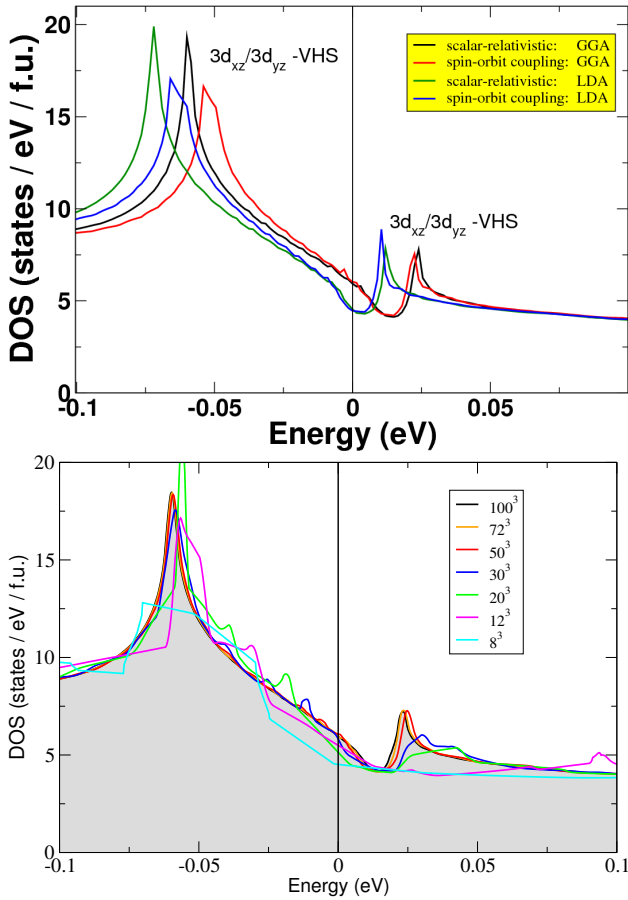


Figure 5 (color online) Upper panel: Calculated total density of states (DOS) for RbFe_2As_2 within scalar relativistic and spin-orbit coupling included LDA and GGA codes, respectively, using a dense mesh of \mathbf{k} -points ($72 \times 72 \times 72$). Notice the pronounced peak-like feature at the bottom of the empty el-pocket near +15 meV, which stems from a generic quasi-2D VHS. Lower panel: Dependence on the number of \mathbf{k} -points for the scalar relativistic GGA calculation.

[114]. The latter has been observed in electron overdoped $\text{BaFe}_{2-x}\text{Co}_x\text{As}_2$ system with $x = 0.11$, above the ordinary spin-stripe phase. The tunneling mode of about 5 THz (≈ 20.4 meV) derived there is fascinating since it nearly coincides with the unknown bosonic mode's energy and suggests the involvement of a strongly anharmonic phonon mode. To confirm such a speculation, it would be desirable to have (i) corresponding EXAFS measurements on a K-122 single crystal and (ii) a deeper theoretical understanding of the suggested double-well potential [140]. In such a scenario, a hybridization with the above discussed excitonic mode or another charge excitation might also occur. Thus inelastic neutron scattering and Raman measurements, as well as isotopic substitutions, might provide a

clearer picture of the nature of this bosonic mode. *Ab initio* DFT calculations are hampered here by the fact that they cannot reproduce the experimental pnictogen position, which is known to affect many physical properties of the FeSCs [141,142]. The previously mentioned unusual dynamical properties of the Fe-As bond provides additional interest to the microscopic consequences for superconductivity and competing phases.

Given all of this, the elucidation of the fate of a corresponding bosonic excitation in Rb- or Cs-122 is a challenge for both experiment and theory.

3.2 Orbital Selective Mott physics versus shifted van Hove singularities. STM measurements [143] on K-122 have observed a VHS related to the $3d_{xz}/3d_{yz}$ orbitals. The observed peak exhibits a rather asymmetric shape resembling our DFT calculations shown in Figs. 5 and 6 for Rb-122 and Cs-122, respectively, but squeezed in width by a factor of two. (Due to a much smaller number of \mathbf{k} -points, some of these VHS and others remained unresolved in Refs. [115, 125].) Moreover, a large discrepancy between experiment and DFT predictions (by a factor of five) appears when comparing its position about the Fermi level, where the experimental features are found closer towards E_F . This trend is in agreement with the predictions of DMFT studies, where the Hubbard U and the Hund's coupling J are more accurately taken into account. In this context, and that of FeSe, an intersite Coulomb interaction V (usually ignored in the DMFT) may also contribute to significant upshifts of the VHS from -250 meV within the DFT to about 25 meV for FeSe, as observed in ARPES measurements. This way the Hubbard U and Hund's ex-

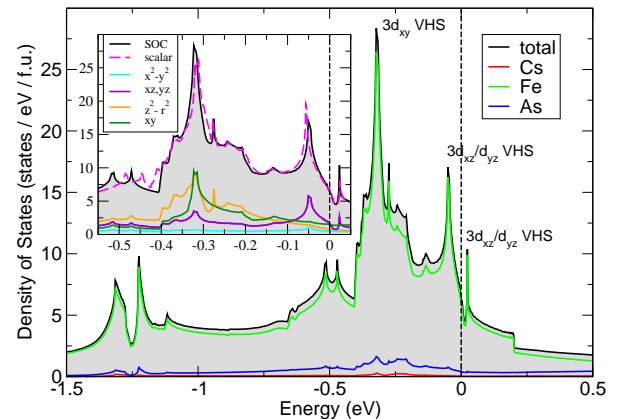


Figure 6 (Color online) Exemplarily calculated total density of states (DOS) for CsFe_2As_2 within full relativistic (SOC) DFT-codes. Inset: orbital-resolved DOS. Notice also the weak VHS near the bottom of the unoccupied el-pocket at about 20 meV discussed in the Sect. 5.1. and mentioned also in the caption of Fig. 5.

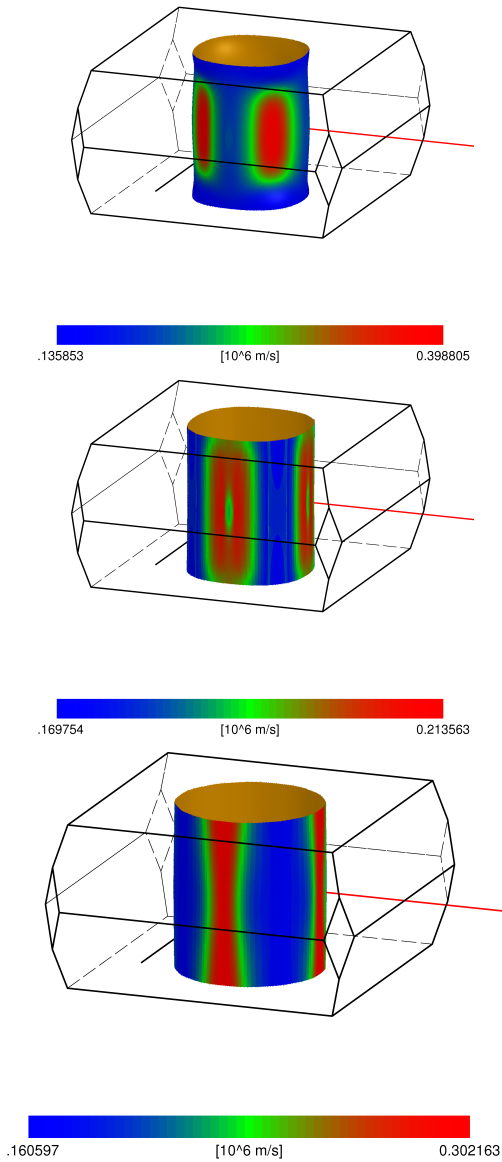


Figure 7 (Color) The three FSS of K-122 centered around the Γ -point of the Brillouin zone (BZ) within DFT. Upper: FSS with dominant $3d_{z^2}$ -character. Middle: FSS with dominant $3d_{xy}$ -character. Lower: FSS with dominant $3d_{xz}/3d_{yz}$ -character. The indicated colors measure the values of the unrenormalized Fermi-velocities.

change J might be somewhat reduced as compared to the values adopted so far. SOC can be important for determining the position of the VHS and the value of the DOS; the two-Fe unit cell accounts for the two different As positions and thus provides an additional SOC between the $3d_{xy}$ and the $3d_{xz}/3d_{yz}$ orbitals at nearest neighbor Fe sites [144].

We will discuss the analogous situation in K-122 (where these effects are more pronounced) and its sister compounds in greater detail elsewhere, along with the

inclusion of new ARPES data and DMFT calculations. As a consequence, the filling ratios of the bands containing the most strongly correlated orbitals are reduced. For completeness, we note that for Cs-122, a VHS close to E_F has not been resolved [145] so far. Instead a turning point in resistivity and specific heat data at $T^* = 13$ K, an anomalous T^3 electronic specific heat below T^* , (pseudo)

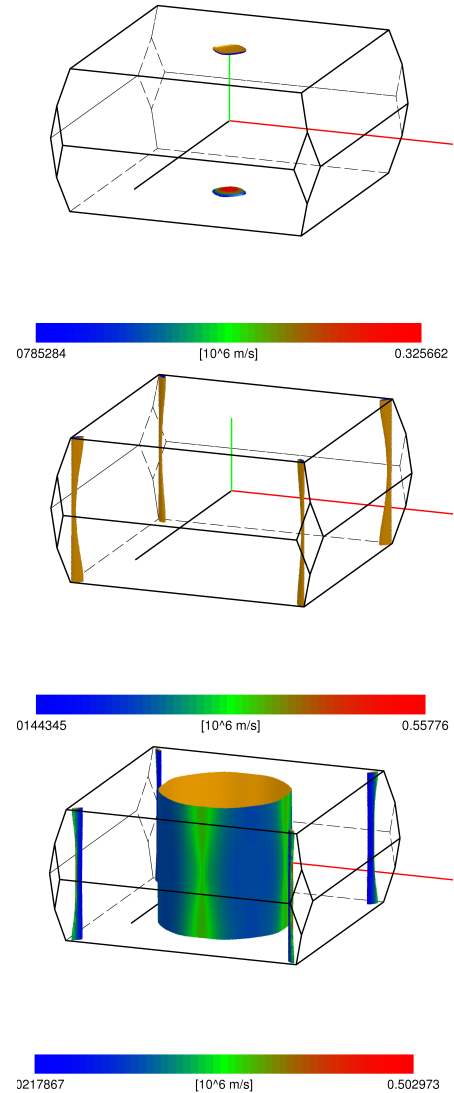


Figure 8 (Color) Upper panel: the closed FSS of K-122 around the Z-point of the BZ with dominant $3d_{z^2}$ character. Middle: The blade-like FSS near the corners of the BZ for K122 according to DFT. Notice the smaller (larger) cross section at $k_z c = 0$ (π), respectively, corresponding to planes which contain the Γ and the Z-points of the BZ. Lower panel: The same for Cs-122 where another highly anisotropic FSS with $3d_{xz}$, d_{yz} orbital character centered around the Γ -point of the BZ corresponding to the lower panel in Fig. 14 is shown, too. The indicated colors measure the values of the unrenormalized Fermi-velocities.

gap-like features at -3.7 meV and 4.7 meV well above $T_c = 2.11$ K, and an unusually large superconducting gap value of 1.2 meV below T_c (pointing possibly to pronounced strong coupling and quantum criticality in the normal state [146]) have been derived from specific heat and STS measurements, respectively. This puzzle of the missing VHS in Cs-122 could be explained by substantial orbital fluctuations related to a locally broken tetragonal symmetry for which a splitting into two components one above and a counterpart below E_F . Alternatively, it might be related to the opening of a pseudogap [118] and or to a charge ordering suggested for an electronically-driven phase separation like in that suggested for Rb-122 [139] at $T = 20$ K. The very observation of charge ordering provides strong arguments against the vicinity of a Mott phase. As an experimental example illustrating that point, we refer to the A15 phase of Cs_3C_{60} [147]. The much lower T_c is attributed to the nodal d -wave character in the present case. The active presence of an incipient band in the superconducting state might explain the smaller anisotropy of H_{c2} as compared to the sister compounds K-122 and Rb-122, despite the largest spacing between the adjacent FeAs-planes due to the biggest ionic radii of the Cs^+ ions.

In addition, some admixture of non-Fermi liquid behavior might be visible in the T -dependent resistivity data, which shows a subquadratic exponent of 1.7 below 10 K. Such an unusual exponent points towards a multiband effect with different Fermi liquid and/or to non-Fermi liquid subsystems. The observation of several distinct characteristic temperatures scales (such as the maximum for the magnetic susceptibility near 50 K, a new scaling of the spin relaxation rate $1/T_1$ below about 85 K, and a further slight kink of the resistivity at about 120 K) also points to a multiband picture that cannot be described using an effective single band model, where a single freezing temperature separates an (extremely) bad metallic and a Fermi liquid phase. We speculate that all these anomalies might be related to the vicinity of a QCP, as proposed in Ref. [115] (ignored in Ref. [11]) and a novel incommensurate magnetic phase with a Fermi surface reconstruction. (See also Fig. 9, where a general phase diagram for the doping dependence of FeSC and the related neighboring magnetic phases is suggested.) Here, the puzzling unresolved VHS might also be affected by Fermi surface reconstruction and broadening effects due to strong spin-orbit coupling and somewhat enhanced correlation effects as compared to K-122.

These considerations show that the positions of the VHS, if visible, can provide a unique possibility to measure the strength of the high-energy el-el interactions. At the same time, the position of the VHS can also influence estimates for the high-energy mass renormalization. For example, a shift and/or the broadening of the VHS can lead to an increase of the DOS at the Fermi energy $N(0)$. As such, a weaker el-el interaction would be required to reproduce the

large Sommerfeld coefficient $\gamma \approx 100$ mJ/mol·K². Using full relativistic GGA-FPLO calculations, the experimental $\gamma \approx 125$ mJ/mol·K² for Rb-122 can be understood without adopting a stronger el-el interaction at variance with Ref. [115].

In order to also explain the record value of $\gamma = 180$ mJ/mol·K² found in the Cs-122 compound, one is left with two options: (i) introduce a strongly increased Hubbard U , as was done in Ref. [115] (which is not very plausible for closely related compounds; alternatively, one should adopt a significant reduction of the screening by almost localized quasi-particles), or (ii) introduce an increased low-energy el-el interaction caused by the closer vicinity of a detrimental QCP. This latter scenario was proposed in Ref. [148, 115]. Here, an increase of the $\lambda_{\text{el-b}}^{\text{low}}$ entering mass renormalization from about 0.5 for K-122 to 1 for Cs-122 could explain the anomalous magnitude of the Sommerfeld coefficient γ . At the same time, this would explain the decrease of T_c if no corresponding increase in the $\lambda_{\text{el-b}}^{\text{low}}$ entering the anomalous self-energy is introduced. (These two contributions are often denoted λ_z and λ_ϕ , respectively.) In this scenario, other effects such as a change of the bosonic spectra favoring competing pairing symmetries could also play some role.

The low-energy bosonic scenario could also be helpful in resolving another puzzle related to the smaller magnetic susceptibility of Cs-122 in comparison to Rb-122 and K-122. A small and even a decreasing Wilson ratio

$$R_W = \frac{4\pi^2 k_B \chi(0)}{3g^2 J(J+1)\gamma(0)} \quad (8)$$

is widely used as a measure of the relative strength of correlation effects. Starting from $R_W(\text{K}) \approx 1$, and using the data from Ref. [118] (Fig. S4 and Tab. S1), one estimates $R_W(\text{Rb})/R_W(\text{K}) \approx 0.727$ and $R_W(\text{Cs})/R_W(\text{K}) \leq 0.394$, while less correlated FeSC exhibit W_R -values in between 2 and 5. This result is in obvious conflict with the notion that stronger correlations are present in Cs-122 and Rb-122 when compared to K-122. Here, we mention that among a large number of known (until the year 2000) heavy-fermion superconductors, only three of them (CeCu_2Si_2 , UPt_3 , and UBe_{13}) exhibit Wilson ratios $W_R \approx 1$ [149]. To the best of our knowledge, there is no system with such a very low $W_R \sim 0.4$ as observed in Cs-122. In general, it is very challenging at present to answer the question about Kondo-like physics presence in these three compounds. To gain more insight into this issue, resistivity measurements well above 300 K with the aim of detecting a maximum of $\rho(T)$ would be helpful. Spin-orbit coupling and an explicit account of As $4p$ orbitals might also be necessary for obtaining a microscopic estimate of the corresponding Kondo exchange coupling J_K between the suggested almost localized $3d_{xy}$ spins and the less correlated $3d_{xz}/3d_{yz}$ and other electrons.

In accord with NMR data for K-122 [118] and especially for NQR data for Rb-122 [139], the FeSC-related

R_W puzzles might be resolved if low-energy *charge* fluctuations were also involved in addition to spin-fluctuations. Since the former are expected to compete with significant on-site correlations on the Fe-sites, we suggest that the latter should mainly involve the much less correlated As $4p$ states. As a result, the unknown phase related to the QCP might be a combined magnetically and weakly charged ordered phase [150] unlike the purely magnetic Mott-phase, as suggested in Ref. [115]. Also, the smaller magnetic moment of $0.97 \mu_B/\text{Fe}$ (compared to 1.48 for K-122 and 1.45 for Rb-122) is unexpected within the slaved spin and DMFT scenarios without taking into account either residual correlations in the As $4p$ states or various intersite Coulomb interactions.

Among the three significant VHS, the Fe $3d_{xz}/d_{yz}$ derived VHS is the closest to E_F and is of special interest here. Its position is between the Γ - and the X -points at the corner of the BZ (i.e. on the nodal line of a $d_{x^2-y^2}$ -wave order parameter). Under these circumstances, critical low-energy spin fluctuations will not provide more glue to SC, but merely enhance the λ_z entering the mass enhancement relative to λ_ϕ entering the anomalous self-energy [54, 55]. This combination would result in a lower T_c , in accord with the experiment. As compared with our first single and two-band calculations in the weak coupling limit [130, 134], by adopting a small difference $\lambda_z - \lambda_\phi$ (as suggested by the small T_c in the vicinity of such a quantum critical point) a strong coupling case with $\lambda_z \sim 2$ might be realized by adopting a reduced frequency of the spin fluctu-

ations in both channels. This way a moderate enhancement of $\lambda_\phi > 1$ can be achieved while conserving the observed low T_c -value. Low- T specific heat and INS measurements like for K-122 [116] are requested for Cs-122 and Rb-122 to confirm such a scenario.

Upon further h-doping, the VHS might come closer still to E_F . This shift could trigger a new incommensurate magnetic phase, distinct from the commensurate Mott phase predicted by orbital-selective Mott scenarios [95]. We note that the situation in (otherwise similar) Sr_2RuO_4 is very different: in Sr_2RuO_4 the VHS of $4d_{xy}$ electrons in the tetragonal phase is located 20 meV below E_F and can be split by external pressure or tension. One of the split components in the orthorhombic phase moves towards E_F , thereby strongly enhancing T_c [151]. We ascribe this opposite effect to the different symmetries of the SCOP in both systems. Regardless, a similar fine-tuning of the VHS-position would be of great interest in our case, providing more insight into the competition of various instabilities.

Returning to Cs-122, we would like to note that strong nematic fluctuations, as suggested recently on the basis of NMR and NQR data [152], would have a similar local splitting effect as magnetic stripe phase fluctuations. In this context, it is very likely that the critical phase I denoted in Fig. 9 includes components from all of the spin, orbital, and charge degrees of freedom. More sophisticated model calculations and additional experimental studies might elucidate which of them is the dominant driving instability. In such a complicated situation, even weak disorder effects might be responsible for slightly different observations reported by various experimental groups. The observation of a disordered glassy magnetic phase coexisting with an only slightly suppressed superconducting state in earlier single crystal samples of K-122 but with a reduced total Sommerfeld coefficient γ , as well as with a significant residual counterpart at $T \rightarrow 0$ [13], is rather remarkable in this context. (Polycrystalline samples also have reduced Sommerfeld [153].) The former might correspond to nonsuperconducting gaps in some of the weakly coupled non-dominant FSS discussed above in the frame of the octet gap picture, and the latter might be related to the quenched superconductivity in weak external magnetic fields reported above. Further studies would be helpful for checking these suggestions. This general nontrivial impurity aspect, as well as the experimental determination of the low- T structures for Rb-122 and Cs-122 including defects, might be very helpful to find a realistic physical scenario for phase I. We argue, however, that this phase is not directly related to a (selected) Mott-phase and involves essentially the less strongly correlated $3d_{xz}$ and $3d_{yz}$ orbitals and the ε (blade) FSS, in particular.

In conclusion, with increasing h-doping novel magnetic and superconducting phases might be found, especially, if a d_{xy} -superconducting phase in the very vicinity to a selective Mott or to an Fe^{3+} state would occur. In the crossover region a gapless $d_{x^2-y^2} + id_{xy}$ phase would also

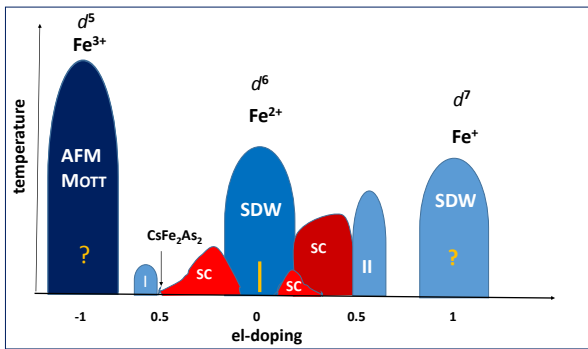


Figure 9 (Color) Suggested general phase diagram of Fe pnictide compounds. Blue: magnetic regions, red: superconducting regions. Phase I - a combined charge, orbital, and spin ordered phase responsible for the vicinity of the critical point as discussed in the text. The yellow line at isovalent or no doping stands for such systems as $\text{Li}(\text{Na})\text{FeAs}$, P-doped $\text{Ba}(\text{Sr})$ -122 and bulk FeSe where the competing magnetic SDW magnetic stripe-phase is absent or strongly suppressed. Phase II has been observed but not been yet characterized experimentally. The outermost hypothetical phase around Fe^+ is our suggestion. The bright red and dark red regions stand for 122 and H doped La-1111 (under pressure) [99] FeSC compounds, respectively.

be a candidate. Present day sophisticated many-body approaches describe qualitatively only some aspects of the normal state properties of FeSC and miss effects such as non-Fermi-liquid behavior in the vicinity of QCPs.

4 Conclusions We have provided strong evidence for the presence of low-energy electron-boson interactions that determine the superconducting and normal state properties of the FeSC. They can be simulated reasonably well by multi-band Eliashberg-theory (also including impurity scattering effects, see Refs. [16, 154]). A phenomenological analysis of normal state and superconducting properties of the FeSC shows that in the retarded glue scenario the el-boson coupling constant averaged over all Fermi surfaces λ_{el-b} is limited by about 1.5. In other words, no strong coupling regime is realized so far. There is also growing evidence for the presence of non-negligible intraband couplings, which stabilize T_c and in some cases. In some cases, this intraband component can even be dominant, as in the case of nodal $4d$ -wave symmetry or an s_{++} SCOP induced by interband impurity scattering. Within such a combined scenario, involving both interband spin-fluctuation mediated interactions and a (not yet well understood) intermediate intraband interaction, even the highest values of T_c observed in el-doped 1111 systems can be at least qualitatively explained.

Acknowledgements The work presented in this review was made possible by the financial support provided by the German Research Foundation (Deutsche Forschungsgemeinschaft (DFG)) through priority program SPP 1458. V.G. is grateful to the DFG through the grant GR4667/1-1 for financial support. The authors thank B. Büchner, R. Hackl, C. Honerkamp and D. Johrendt for initiating this priority program and for discussions. Further thanks to J. van den Brink, D. Efremov, O. Dolgov, S. Borisenko, S. Backes, J. Tomczak, L. de Medici, R. Valenti, S. Biermann, G. Kotliar, A. Chubukov, M. Dressel, R. Thomale, J. Schmalian, H. Kühne, A. Boris, A. Charetta, A. Yaresko, H.-J. Klauss, G. Fuchs, R. Schuster, C. Geipel, N.M. Plakida, K. Kikoin, F. Hardy, S. Khim, P. Mydosh, I. Morozov, and S. Aswartham for numerous and helpful discussions.

References

[1] Y. Kamihara, T. Watanabe, M. Hirano, and H. Hosono, *J. Am. Chem. Soc.* **128**, 10012 (2006).
 [2] Y. Kamahara, T. Watanabe, M. Hirano, and H. Hosono, *J. Am. Chem. Soc.* **130**, 3296 (2008).
 [3] D. Johnston, *Adv. Phys.* **59**, 803 (2010).
 [4] S. J. Paglione and R. Greene, *Nat. Phys.* **6**, 645 (2010).
 [5] G. R. Stewart, *Rev. Mod. Phys.* **83**, 1589 (2011).
 [6] P. J. Hirschfeld, *Comptes Rendus Physique* **17**, 197 (2016).
 [7] N. Mannella, *J. Phys.: Condens. Matter* **26**, 473202 (2014).
 [8] L. Boeri, O. Dolgov, and A. Golubov, *Phys. Rev. Lett.* **101**, 026403 (2008).
 [9] L. Rettig, R. Cortes, H. Jeevan, P. Gegenwart, T. Wolf, J. Fink, and U. Bovensiepen, *New J. Phys.* **15**, 083023 (2013).

[10] F. Hardy, R. Eder, M. Jackson, A. Dai, C. Paulsen, T. Wolf, P. Burger, A. Boehmer, P. Schweiss, P. Adelmann, R. Fisher, and C. Meingast, *J. Phys. Soc. Jpn.* **83**, 014711 (2013).
 [11] F. Hardy, A. Böhmer, L. de Medici, M. Capone, G. Giovannetti, R. Eder, L. Wang, M. He, T. Wolf, P. Schweiss, R. Heid, A. Herbig, P. Adelmann, R. Fisher, and C. Meingast, *Phys. Rev. B* **94**, 205113 (2016).
 [12] J. P. Reid, M. Tanatar, A. Juneau-Fecteau, R. Gorton, S. de Cortret, N. Doiron-Leyraud, T. Saito, H. Fukuzawa, Y. Kohoni, K. Kihour, C. Lee, A. Iyo, H. Eisaki, R. Prozorov, and L. Taillefer, *Phys. Rev. Lett.* **109**, 087001 (2012).
 [13] V. Grinenko, S. L. Drechsler, M. Abdel-Hafiez, S. Aswartham, A. Wolter, S. Wurmehl, C. Hess, K. Nenkov, G. Fuchs, D. Efremov, B. Holzapfel, J. van den Brink, and B. Buechner, *Phys. Stat. Sol. B* **250**, 593 (2013).
 [14] H. Kim, M. Tanatar, Y. Liu, Z. Sims, C. Zhang, P. Dai, T. Lagasso, and R. Prozorov, *Phys. Rev. B* **89**, 174519 (2014).
 [15] Q. Wang, J. Park, F. Y., Y. Shen, Y. Hao, B. Pam, J. Lynn, A. Ivanov, S. Chi, M. Matsuda, H. Cao, R. Birgenau, D. Efremov, and J. Zhao, *Phys. Rev. Lett.* **116**, 197004 (2016).
 [16] D. Efremov, V. Grinenko, O. Dolgov, and S. L. Drechsler, to be published (2017).
 [17] Z. P. Yin, K. Haule, and G. Kotliar, *Nature Materials* **10**, 932 (2011).
 [18] L. de Medici, G. Giovannetti, and M. Capone, *Phys. Rev. Lett.* **112**, 177001 (2014).
 [19] S. Johnston, M. Abdel-Hafiez, L. Harnagea, V. Grinenko, D. Bombor, Y. Krupskaya, C. Hess, S. Wurmehl, A. U. B. Wolter, B. Buechner, H. Rosner, and S. L. Drechsler, *Physical Review B* **89**, 134507 (2014).
 [20] L. Rademaker, Y. Wang, T. Berlijn, and S. Johnston, *New Journal of Physics* **18**, 022001 (2016).
 [21] Y. Wang, K. Nakatsukasa, L. Rademaker, T. Berlijn, and S. Johnston, *Supercond. Sci. Technol.* **29**, 054009 (2016).
 [22] L. Benfatto, E. Cappelluti, and C. Castellani, *Phys. Rev. B* **80**, 214522 (2009).
 [23] O. Dolgov, D. Efremov, M. Korshunov, A. Charnukha, A. Boris, and A. Golubov, *J. of Supercond. and Novel Magnet.* **26**, 2637–2640 (2013).
 [24] G. Umbarino and D. Daghero, *J. Phys. Condens. Mat.* **27**, 435701 (2015).
 [25] G. Umbarino, M. Tortello, D. Daghero, and R. Gonelli, *Phys. Rev. B* **80**, 172503 (2009).
 [26] G. Umbarino, S. Galasso, and A. Sanna, *J. Phys. Cond. Mat.* **25**, 205701 (2013).
 [27] G. Umbarino, *Phys. Rev. B* **83**, 092508 (2011).
 [28] S. L. Drechsler, S. Borisenko, S. Khim, V. Grinenko, G. Fuchs, S. Aswartham, S. Wurmehl, B. Büchner, S. Backes, R. Valenti, J. Tomczak, I. Morozov, and H. Rosner, Abstracts of the International Workshop on Iron-based superconductors, DFG SPP 1458 pp. P. 16, Munich, Germany, September 13–16 (2016).
 [29] A. van Roekeghem, P. Richard, H. Ding, and S. Biermann, *Comptes Rendus Physique* **17**, 140 (2015).

- [30] I. I. Mazin, D. J. Singh, M. D. Johannes, and M. H. Du, *Phys. Rev. Lett.* **101**, 057003 (2008).
- [31] D. J. Scalapino, *Rev. Mod. Phys.* **84**, 1383 (2012).
- [32] H. Kontani and S. Onari, *Phys. Rev. Lett.* **104**, 157001 (2010).
- [33] J. Kang and R. M. Fernandes, *Phys. Rev. Lett.* **117**, 217003 (2016).
- [34] M. Capone, C. Castellani, and M. Grilli, *Advances in Condensed Matter Physics* **2010**, 920860 (2010).
- [35] S. Mandal, R. E. Cohen, and K. Haule, *Phys. Rev. B* **82**, 020506 (2014).
- [36] S. Coh, M. L. Cohen, and S. G. Louie, *New J. Phys.* **17**, 073027 (2015).
- [37] S. Coh, M. L. Cohen, and S. G. Louie, *Phys. Rev. B* **94**, 104505 (2016).
- [38] G. Sawatzky, I. Elfimov, J. van den Brink, and J. Zaanen, *EPL* **86**, 17006 (2009).
- [39] S. L. Drechsler, H. Rosner, M. Grobosch, G. Behr, F. Roth, G. Fuchs, K. Koepfner, R. Schuster, J. Malek, S. Elgazzar, M. Rotter, D. Johrendt, H. H. Klauss, B. Buechner, and M. Knupfer, *arXiv:0904.0827v1* (2009).
- [40] M. L. Kulić and A. A. Haghighirad, *EPL* **870** (2009).
- [41] S. Johnston, C. Monney, V. Bisogni, K. J. Zhou, R. Kraus, G. Behr, V. Strocov, J. Mlek, S. L. Drechsler, T. Geck J. Schmitt., and J. van den Brink, *nature comm.* **7**, 10563 (2016).
- [42] L. Rettig, S. Mariager, A. Ferrer, S. Grübel, J. Johnson, J. Rittmann, T. Wolf, S. Johnson, G. Ingold, P. Beaud, and U. Staub, *Phys. Rev. Lett.* **15**, 067402 (2015).
- [43] C. Cantoni, A. McGuire, B. Saparov, A. May, T. Keiber, F. Bridges, A. Sefat, and B. Sales, *Advanced Materials* **27**, 2715 (2015).
- [44] V. Barzykin and L. Gor'kov, *Phys. Rev. B* **79**, 134510 (2009).
- [45] M. Widom and K. Quander, *J. Supercond. & Novel Magnet.* **29**, 685 (2016).
- [46] P. Kumar, A. Kumar, S. Saha, D. Muthu, J. Prakash, U. Waghmare, A. Ganguli, and A. Sood, *J. Phys. Condens. Mat.* **22**, 254402 (2010).
- [47] A. Kumar, P. Kumar, V. Umesh, U. Waghmare, and A. Sood, *J. Phys. Condens. Mat.* **22**, 385701 (2010).
- [48] P. Kumar, D. Muthu, L. Hanaragea, S. Wurmehl, B. Büchner, and A. Sood, *J. Phys. Condens. Mat.* **26**, 305403 (2014).
- [49] R. Zeyher and M. L. Kulić, *Phys. Rev. B* **53**, 2850 (1996).
- [50] J. Lee, F. Schmitt, R. Moore, S. Johnston, Y. T. Cui, W. Li, M. Yi, Z. Liu, M. Hashimoto, Y. Zhang, D. Lu, T. Devereaux, D. H. Lee, and Z. H. Shen, *Nature* **515**, 245 (2014).
- [51] T. A. Maier, D. Poiblanc, and D. J. Scalapino, *Phys. Rev. Lett.* **100**, 237001 (2008).
- [52] H. Iwasawa, Y. Yoshida, I. Hase, S. Koikegami, H. Hyashi, J. Jiang, K. Shimada, M. Hirano, H. Namatame, M. Taniguchi, and Y. Aiura, *Phys. Rev. Lett.* **105**, 226406 (2010).
- [53] H. Iwasawa, Y. Yoshida, M. Hirano, I. Hase, K. Shimada, H. Namatame, M. Taniguchi, and Y. Aiura, *Scient. Rep.* **3**, 1930 (2013).
- [54] N. Bulut and D. J. Scalapino, *Phys. Rev. B* **54**, 14971 (1996).
- [55] S. Johnston and T. P. Devereaux, *Phys. Rev. B* **81**, 214512 (2010).
- [56] Y. Dai, H. Miao, L. Xing, X. Wang, C. Jin, H. Ding, and C. Homes, *Phys. Rev. B* **93**, 054508 (2016).
- [57] B. Cheng, B. F. Hu, R. Y. Chen, G. Xu, P. Zheng, J. L. Luo, and N. L. Wang, *Phys. Rev. B* **86**, 134503 (2012).
- [58] S. L. Drechsler, F. Roth, M. Grobosch, R. Schuster, K. Koepfner, H. Rosner, G. Behr, M. Rotter, D. Johrendt, B. Buechner, and M. Knupfer, *Physica C* **470**, S332 (2010).
- [59] E. Maksimov, A. Karakozov, B. Gorshunova, Y. Ponomareb, and M. Dressel, *Phys. Rev. B* **84**, 174504 (2011).
- [60] Y. Wu, N. Barisić, P. Kallina, A. Faridian, B. Gorshunov, N. Drichko, L. J. Li, X. Lin, G. H. Cao, Z. A. Xu, N. L. Wang, and M. Dressel, *Phys. Rev. B* **81**, 100512(R) (2010).
- [61] A. Charnukha, D. Präpper, T. Larkin, D. Sun, Z. Li, C. Lin, T. Wolf, B. Keimer, and A. Boris, *Phys. Rev. B* **88**, 184511 (2013).
- [62] Y. Dai, A. Akrap, L. Bud'ko, P. Canfield, and C. Homes, *Phys. Rev. B* **94**, 195142 (2016).
- [63] A. Tytarenko, Y. Huang, A. de Visser, S. Johnston, and E. van Heumen, *Sci. Rep.* **5**, 12421 (2015).
- [64] E. van Heumen, Y. Huang, S. de Jong, A. B. Kuzmenko, M. S. Golden, and D. van der Marel, *Europhys. Lett.* **90**, 37005 (2010).
- [65] L. Benfatto, E. Cappelluti, L. Ortenzi, and L. Boeri, *Phys. Rev. B* **83**, 224514 (2011).
- [66] J. Diel, S. Backes, D. Guterding, H. Jeschke, and V. Roser, *Phys. Rev. B* **90**, 085110 (2014).
- [67] P. Materne, S. Kamusella, R. Sarkar, T. Goltz, J. Spelling, M. Maeter, L. Harnagea, S. Wurmehl, B. Buechner, C. Luetkens H. Timm., and H. H. Klauss, *Phys. Rev. B* **92**, 134511 (2015).
- [68] S. L. Drechsler, M. Grobosch, K. Koepfner, G. Behr, A. Koehler, J. Werner, A. Kondrat, N. Leps, C. Hess, R. Klingeler, R. Schuster, B. Buechner, and M. Knupfer, *Phys. Rev. Lett.* **101**, 257004 (2008).
- [69] Z. Guguchia, R. Khasanov, Z. Bukowski, F. von Rohr, M. Medarde, P. Biswas, H. Luetkens, A. Amato, and E. Morenzoni, *Phys. Rev. B* **93**, 094513 (2016).
- [70] A. Georges, L. de' Medici, and J. Mravlje, *Annual Reviews of Condensed Matter Physics* **4**, 137 (2013).
- [71] L. de Medici and M. Capone, *arXiv:1607.08468* (2016).
- [72] V. Brouet, P. LeBeuf, P. H. Lin, J. Mansart, A. Taleb-Ibrahimi, P. LeFevre, F. Bertrand, A. Forget, and D. Colson, *Phys. Rev. B* **93**, 085137 (2016).
- [73] A. Rokeghem, L. Vaugier, H. Jiang, and S. Biermann, *Phys. Rev. B* **94**, 125147 (2016).
- [74] D. Guterding, S. Backes, M. Tomic, H. Jeschke, and R. Valenti, *phys. stat. sol. (b)* (in press), *arXiv:1606.04411v1* (2016).
- [75] S. Backes, M. Tomic, H. Jeschke, and R. Valenti, *Phys. Rev. B* **92**, 195128 (2015).
- [76] J. Carbotte, *Rev. Mod. Phys.* **62**, 1027 (1990).
- [77] P. W. Anderson, *Science* **316**, 1705 (2007).

- [78] G. Fuchs, S. L. Drechsler, N. Kozlova, G. Behr, A. Koehler, J. Werner, K. Nenkov, R. Klingeler, J. Hamann-Borrero, C. Hess, A. Kondrat, M. Grobosch, A. Narduzzo, M. Knupfer, J. Freudenberger, B. Buechner, and L. Schultz, *Phys. Rev. Lett.* **101**, 237003 (2008).
- [79] G. Fuchs, S. L. Drechsler, N. Kozlova, M. Bartkowiak, J. E. Hamann-Borrero, G. Behr, K. Nenkov, H. H. Klauss, H. Maeter, A. Amato, H. Luetkens, A. Kwadrin, R. Khasanov, J. Freudenberger, A. Koehler, M. Knupfer, E. Arushanov, H. Rosner, B. Buechner, and L. Schultz, *New Journal of Physics* **11**, 075007 (2009).
- [80] A. Charnukha, O. Dolgov, A. Golubov, Y. Matiks, D. Sun, C. Lin, B. Keimer, and A. Boris, *Phys. Rev. B* **84**, 174511 (2011).
- [81] P. Popovich, A. V. Boris, O. V. Dolgov, A. A. Golubov, D. L. Sun, C. T. Lin, R. K. Kremer, and B. Keimer, *Phys. Rev. Lett.* **105**, 027003 (2010).
- [82] D. Evtushinsky, V. Zabolotnyy, L. Harnagea, A. Yaresko, S. Thirupathiah, A. Kordyuk, J. Maletz, S. Aswartham, S. Wurmehl, E. Rienks, R. Follath, B. Buechner, and B. S. V., *Phys. Rev. B* **87**, 094501 (2013).
- [83] Y. B. Shi, Y. B. Huang, X. P. Wang, X. Shi, A. V. Roekeghem, W. L. Zhang, N. Xu, P. Richard, Q. T., E. Rienks, S. Thirupathiah, K. Zhao, C. Q. Jing, M. Shi, and H. Ding, *Chin. Phys. Lett.* **31**, 067403 (2014).
- [84] J. Hwang, *J. Phys. Condens. Matter* **28**, 125709 (2016).
- [85] G. Derondeau, F. Bisti, J. Braun, V. Rogalev, M. Shi, T. Schmitt, J. Ma, H. Ding, H. Ebert, V. Strocov, and J. Minar, arXiv:1606.08977v1 (2016).
- [86] S. Johnston and *et al.*, in preparation (2016).
- [87] P. Hlobil, J. Jandke, W. Wulfhekel, and J. Schmalian, arXiv:1603.05288v2 (2016).
- [88] J. Schmalian, private comm. (2016).
- [89] D. Inosov, J. Park, A. Charnukha, Y. Li, A. Boris, B. Keimer, and V. V. Hinkov, *Phys. Rev. B* **83**, 14520 (2011).
- [90] C. Kant, J. Deisenhofer, A. Günther, F. Schrettle, M. Rotter, D. Johrendt, and A. Loidl, *Phys. Rev. B* **81**, 014529 (2009).
- [91] F. Ma, Z. Y. Lu, and T. Xiang, *Front. Phys. China* **5**, 150 (2010).
- [92] M. Tortello, D. Daghero, G. Ummarino, V. Stepanov, J. Jiang, J. Wiss, E. Hellstrom, and R. Gonelli, *Phys. Rev. Lett.* **105**, 237002 (2010).
- [93] L. Ortenzi, E. Cappelluti, L. Benfatto, and L. Pietronero, *Phys. Rev. Lett.* **103**, 046404 (2009).
- [94] L. Benfatto and E. Cappelluti, *Phys. Rev. B* **83**, 104516 (2011).
- [95] A. Linscheid, S. Maiti, Y. Wang, S. Johnston, and P. Hirschfeld, arXiv:1603.03739v1 (2016).
- [96] A. Chubukov, I. Eremin, and D. Efremov, arXiv:1601.01678v1 (2016).
- [97] D. Valentini, D. van der Marel, and C. C. Berthod, arXiv:1601.04521v2 (2016).
- [98] A. Karakozov, S. Zapf, B. Gorshunova, Y. Ponomarev, M. Magnitskaya, E. Zhukova, A. Prokhorov, V. Anzin, and S. Hayndl, *Phys. Rev. B* **90**, 014506 (2014).
- [99] N. Kawaguchi, S. Fujiwara, S. Iimura, S. Matsuishi, and H. Hosonol, arXiv:1609.04957v1 (2016).
- [100] V. Ginzburg and D. Kirzhnits (eds.), Maksimov, E.G. and Karakozov, A.E. in *"High Temperature Superconductivity"* Chapt. 7 (New York: Consultant Bureau, 1982).
- [101] P. Fulde, in *"Handbook on the Physics and Chemistry of Rare Earths"* ed. by Gscheidner Jr., K.A., vol. 2, p. 295 (North-Holland, Amsterdam, 1978).
- [102] Y. Naidyuk, O. Kvitnitskaya, D. Yanson, G. Fuchs, K. Nenkov, A. Wälte, G. Behr, D. Souptel, and S. L. Drechsler, *Phys. Rev. B* **76**, 014520 (2007).
- [103] Y. Xiao, M. Zbiri, R. Downie, J. W. G. Bos, T. Brückel, and T. Chatterji, *Phys. Rev. B* **88**, 214419 (2013).
- [104] Q. Y. W. *et al.*, *Chin. Phys. Lett.* **29**, 037402 (2012).
- [105] H. Wang, A. Kreisel, P. Hirschfeld, and V. Mishra, arXiv:1606.02198v1 (2016).
- [106] W. Kyung, S. Huh, Y. Koh, K. Y. Choi, M. Nakajima, H. Eisaki, J. Denlinger, S. K. Mo, C. Kim, and Y. Kim, *Nature Materials* **15**, 1233 (2016).
- [107] S. Choi, W. J. Jangi, H. J. Lee, J. Ok, H. Choi, A. Lee, A. Akbari, K. Nakatsukasa, Y. Semertzidis, Y. Bang, S. Johnston, J. Kim, and J. Lee, arXiv:1608.00886v2 (2016).
- [108] M. L. Kulić and O. Dolgov, arXiv:1607.00843 (2016).
- [109] Y. Inada and K. Nasu, *J. Phys. Soc. Jpn.* **61**, 4511 (1992).
- [110] J. K. Freericks, M. Jarrell, and G. D. Mahan, *Phys. Rev. Lett* **77**, 4588 (1996).
- [111] J. Chang, I. Eremin, and P. Thalmeier, *New Jour. of Phys.* **11**, 055068 (2009).
- [112] L. Bergmann, E. Cappelluti, and C. Castellani, *Phys. Rev. B* **7**, 480 (2009).
- [113] D. Rainer, G. Bergmann, and U. Eckhardt, *Phys. Rev. B* **8**, 5324 (1973).
- [114] V. Ivanov, A. Ivanov, A. P. Menushenkov, B. Joseph, and A. Bianconi, *J. Supercond. Nov. Mat.* **29**, 3035 (2016).
- [115] F. Eilers, K. Grube, D. Zocco, T. Wolf, M. Merz, P. Schweiss, R. Heid, R. Eder, R. Yu, J. X. Zhu, Q. Si, T. Shibauchi, and H. Hilbert v. Löhneysen, *Phys. Rev. Lett.* **116**, 237003 (2016).
- [116] C. H. Lee, K. Kihou, H. Kawano-Furukawa, T. Saito, A. Iyo, H. Eisaki, H. Fukazawa, Y. Kohori, K. Suzuki, H. Usui, K. Kuroki, and K. Yamada, *Phys. Rev. Lett.* **116**, 067003 (2011).
- [117] M. Zingl, E. Assmann, P. Seth, I. Krivenko, and M. Aichhorn, *Phys. Rev. B* **94**, 045130 (2016).
- [118] Y. Wu, D. Zhao, A. Wang, N. Wang, Z. Xiang, X. Luo, T. Wu, and X. Chen, *Phys. Rev. Lett.* **116**, 147001 (2016).
- [119] K. Koepf and H. Eschrig, *Phys. Rev. B* **59**, 1743 (1999).
- [120] I. Opahle, K. Koepf, and H. Eschrig, *Phys. Rev. B* **60**, 14035 (1999).
- [121] J. P. Perdew, B. K., and M. Ernzerhof, *Phys. Rev. Lett* **77**, 3865 (1996).
- [122] H. Eschrig, M. Richter, and I. Opahle, *Theoretical and Computational Chemistry* **13**, 733 (2004).
- [123] Z. Wang, A. Wang, X. Hong, J. Zhang, B. Pan, P. Pan, Y. Xu, X. Luo, X. Chen, and S. Li, *Phys. Rev. B* **91**, 024502 (2015).
- [124] S. Khim, S. Aswartham, V. Grinenko, D. Efremov, C. Blum, F. Steckel, D. Gruner, A. Wolter, S. L. Drechsler, C. Hess, S. Wurmehl, and B. Buechner, *phys. stat. sol. (b)* **xxx**, in press (2016).

- [125] Y. Mizukami, Y. Kawamoto, Y. Shimoyama, S. Kurata, H. Ikeda, T. Wolf, D. Zocco, K. Grube, and H. Löhneysen, *Phys. Rev. B* **94**, 024508 (2016).
- [126] T. Terashima, M. Kimata, H. Satsukawa, A. Harada, K. Hazama, S. Uji, H. Harima, G. F. Chen, J. L. Luo, and N. L. Wang, *J. Phys. Soc. Jpn.* **78**, 063702 (2009).
- [127] F. Eilers, PhD-Thesis: Superconductivity and electronic structure of KFe_2As_2 , RbFe_2As_2 , and CsFe_2As_2 probed by thermal expansion and magnetostriction at very low temperatures (University Press, Stuttgart, 2014).
- [128] O. Vafek and A. Chubukov, arXiv:1611.05802v1 (2016).
- [129] V. Grinenko, D. V. Efremov, S. L. Drechsler, S. Aswartham, D. Gruner, M. Roslova, I. Morozov, K. Nenkov, S. Wurmehl, A. Wolter, B. Holzapfel, and B. Buechner, *Phys. Rev. B* **89**, 060504 (2014).
- [130] M. Abdel-Hafiez, V. Grinenko, S. Aswartham, I. Morozov, M. Roslova, O. Vakaliuk, S. Johnston, D. V. Efremov, J. van den Brink, H. Rosner, M. Kumar, C. Hess, S. Wurmehl, A. Wolter, B. Buechner, E. Green, J. Wosnitzer, P. Vogt, A. Reifenberger, C. Enss, M. Hempel, R. Klingeler, and S. L. Drechsler, *ibid.* **87**, 180507 (2013).
- [131] K. Okazaki, Y. Ota, Y. Kotani, W. Malaeb, Y. Ishida, S. T. Kiss, W. S. C. T. Chen, K. Kihou, and *et al.*
- [132] Y. Ota, K. Okazaki, Y. Kotani, T. Shimojima, W. Malaeb, S. Watanabe, C. T. Chen, K. Kihou, C. Lee, A. Iyo, and *et al.*, *Phys. Rev. B* **89**, 081103 (2014).
- [133] Y. Amano, M. Ishihara, M. Ichioka, N. Nakai, and K. Machida, *Phys. Rev. B* **91**, 144513 (2015).
- [134] V. Grinenko, W. Schottenhamel, A. U. B. Wolter, D. V. Efremov, S. L. Drechsler, S. Aswartham, M. Kumar, S. Wurmehl, M. Roslova, I. V. Morozov, B. Holzapfel, B. Buechner, E. Ahrens, S. I. Troyanov, S. Koehler, E. Gati, S. Knoener, N. H. Hoang, M. Lang, F. Ricci, and G. Profeta, *Physical Review B* **90**, 094511 (2014).
- [135] T. Yoshida, S. S. Ideta, I. Nishi, A. Fujimori, M. Yi, S. Moore, R. G. Mo., D. H. Lu, S. Z. Shen, Z. Hussain, K. Kihou, P. Shirage, H. Kito, C. H. Lee, A. Iyo, H. Eisaki, and H. Harima, *Front. Phys.* **2**, 17 (2014).
- [136] Y. Naidyuk, O. E. Kvitnitskaya, N. Gamayunova, L. Boeri, S. Aswartham, S. Wurmehl, B. Buechner, D. Efremov, G. Fuchs, and S. L. Drechsler, *Phys. Rev. B* **90**, 094505 (2014).
- [137] S. Avci, O. Chmaissem, D. Ghung, S. Rosenkrans, E. Goremychkin, J. Castellán, I. Todorov, J. Schlueter, H. Claus, A. Daoud-Aladine, D. Khalyavin, M. Kanatshidis, and R. Osborn, *Phys. Rev. B* **85**, 184507 (2012).
- [138] P. S. Wang, P. Zhou, J. Dai, J. Zhang, X. X. Ding, P. Lin, H. Wen, B. Normand, R. Yu, and W. Yu, *Phys. Rev. B* **93**, 085129 (2016).
- [139] E. Civardi, M. Moroni, M. Babij, X. Bukowsky, and P. Caretta, arXiv:04532v1 (2016).
- [140] C. P. J. Adolphs and M. Berciu, *Phys. Rev. B* **90**, 085149 (2014).
- [141] K. Kuroki, Proceedings SNS2010, arXiv:1008.2286 (2010).
- [142] Y. Mizuguchi, Y. Hara, K. Deguchi, S. S. Tsuda, T. Yamaguchi, K. Takeda, H. Kotegawa, H. Tou, and Y. Takano, *Supercond. Sc. and Techn.* **5**, 054013 (2010).
- [143] D. Fang, X. Shi, Z. Du, P. Richard, H. Yang, X. Wu, P. Zhang, T. Qian, X. Ding, Z. Wang, T. Kim, M. Hoesch, A. Wang, X. Chen, J. Hu, H. Ding, and H. H. Wen, *Phys. Rev. B* **92**, 144513 (2015).
- [144] R. Fernandes and A. Chubukov, arXiv:1607.00865v1 (2016).
- [145] H. Yang, J. Xing, Z. Du, X. Yang, H. Lin, D. Fang, X. Zhu, and H. H. Wen, *Phys. Rev. B* **88**, 224516 (2012).
- [146] J. Zaanen, *Phys. Rev. B* **80**, 212502 (2009).
- [147] H. Alloul, P. Wzietek, T. Mito, D. Pontiroli, M. Aramini, M. Rico, and E. Elkaim, arXiv:1610.00513 (2016).
- [148] J. Dong, S. Zhou, T. Guan, H. Zhang, Y. Dai, X. Qiu, X. Wang, Y. He, X. Chen, and S. Li, *ibid.* **104**, 087005 (2010).
- [149] H. Radousky, *Magnetism in heavy fermion compounds*, 2000.
- [150] S. L. Drechsler, J. Malek, H. Eschrig, H. Rosnerr, and R. Hayn, *J. of Supercond.* **10**, 393 (1997).
- [151] H. Taniguchi, K. Nishimura, S. Goh, S. Yonezawa, and Y. Maeno, *J. Phys. Soc. Jpn.* **84**, 014707 (2015).
- [152] J. Li, D. Zhao, Y. Wu, S. Li, D. Song, L. Zheng, N. Wang, X. Luo, Z. Sun, T. Wu, and X. Chen, arXiv:1611.04694v1 (2016).
- [153] H. Fukazawa, Y. Yamada, K. Kondo, T. Saito, Y. Kohori, K. Kuga, Y. Matsumoto, S. Nakatsuji, H. Kito, P. Shirage, K. Kihou, N. Takeshita, C. H. Lee, A. Iyo, and H. Eisaki, *J. Phys. Soc. Jpn.* **78**, 083712 (2009).
- [154] M. M. Korshunov, Y. Togushova, and O. Dolgov, *Phys. Usp.* **186**, 1315 (2016).